Combined effects of interphase-boundary advection and migration during particle growth or dissolution

Frank Montheillet, Asdin Aoufi, David Piot

Combined effects of interphase-boundary advection and migration during particle growth or dissolution

F. Montheillet[a,1*], A. Aoufi[a], D. Piot[a]

[a]Mines Saint-Etienne, Univ Lyon, CNRS, UMR 5307 LGF, Centre SMS,
158 cours Fauriel, 42023 Saint-Etienne Cedex2, France

[1]CNRS emeritus

montheil@emse.fr, aoufi@emse.fr, david.piot@mines-stetienne.fr

Abstract: The growth or dissolution of a particle under compression or simple shear is investigated by means of an analytical approach. The changes in shape and size of the particle are determined by the combination of two interphase movements: *migration* (with respect to matter) and *advection* (driven by the moving matter). The problem is solved by an indirect original method, where the particle surface is derived as the envelope of a family of straight lines (2D) or planes (3D), which leads to closed form parametric equations. It is shown that the shapes of deformed particles are close to, and can be fitted by, ellipsoids. The equivalent strain dependence of the aspect ratio is similar for both investigated loading paths: particle flattening or elongation is reduced by growth, and conversely increased during dissolution. Finally, upon growth from a zero initial radius, the aspect ratio is a function of the applied strain only, which is contrary to intuition.

Keywords: boundary migration, particle growth, dissolution, uniaxial compression, simple shear, grain growth, recrystallization, analytical modeling.

1. Introduction

Temperature holding of a polycrystal generally leads to grain growth (Fig. 1a). The same type of phenomenon may occur in materials containing second phase particles, where the latter nucleate, grow, or dissolve during heat treatment according to chemical equilibrium. This is achieved by grain or interface boundary *migration*, which is a (non-material) movement with respect to matter. It is basically a diffusion process, which endows boundaries with a mobility. By contrast, when a material is deformed at room temperature or more generally in conditions such that mobility can be neglected (*e.g.* at high strain rates), grain and interphase boundaries move simply because they are driven by matter (Fig. 1b). This second type of motion can be considered as a type of *advection*. In hot deformation of metals, migration and advection of boundaries combine together in more or less complex ways, thus influencing the shape as well as size changes of grains and second phase particles during straining. Diffusion assisted grain or particle fragmentation during deformation as well as static grain growth and dynamic recrystallization or dynamic precipitation are likely to be affected [Montheillet and Piot, 2017].

The shape change of an inhomogeneity in a matrix submitted to any prescribed velocity field has long been investigated, for instance in the relatively simple case of spheroidal voids (considered as special inclusions) [Budianski et *al.*, 1982] or inclusions [Gilormini and Montheillet, 1986]. In such models, the particle interface is assumed to remain fixed with respect to matter, which means that the mass of the particle does not change with time. On the other side, grain growth during solidification (liquid matrix) as well as recrystallization and grain growth in a solid matrix have been addressed by various methods, such as analytical approaches [*e.g.* Burke and Turnbull, 1952], cellular automata [Hesselbarth and Göbel, 1991], vertex method [Maurice and

Humphreys, 1998], phase field method [Moelans *et al.*, 2013], and level set-finite element (LS-FE) computations [Bernacki *et al.*, 2009]. In all cases, however, *static* grain growth or recrystallization phenomena have been considered, *i.e.* occurring in a non-deforming material (which is the specific meaning of static here). In some cases, the influence of elastic strains has also been taken into consideration [Duddu *et al.*, 2011]. Only recently, complex semi-analytical [Piot *et al.*, 2018; Maire *et al.*, 2018] and LS-FE [Maire *et al.*, 2017; Ruiz Sarrazola, Maire *et al.*, 2020; Ruiz Sarrazola, Pino Muñoz *et al.*, 2020] approaches have been applied to the case of *dynamic* recrystallization, leading to first results about the influence of large plastic strains on the growth (or shrinkage) of grains. It has also been shown that a simple one-dimensional model combining plastic strain and grain-boundary migration allows to estimate the migration rate from the measurement of the average grain thickness after hot compression [Gourdet and Montheillet, 2002].

In the present article, an analytical model is proposed for predicting the kinematics of growing or shrinking particles in a material submitted to simple velocity fields up to large strains. Closed-form equations for the current shape and size of a particle are obtained, and specific effects of boundary migration are highlighted.

2. Overview of the model

In the following, an isolated particle in a homogeneous matrix is considered with initial spherical shape of radius r_0 (possibly zero). The velocity (advection) field $\boldsymbol{v_c}$ is assumed uniform, which means that perturbations induced by the presence of the inclusion are negligible. This condition is fulfilled for instance in the Taylor (uniform strain rate) assumption. Although the model is more general, two specific strain paths will be addressed, *viz.* uniaxial compression and simple shear, corresponding to

classical compression and torsion experiments, respectively. The main driving force for migration is the decrease of chemical free enthalpy associated with the phase transformation. The energy density is assumed homogeneous within the particle as well as in the surrounding matrix, which involves a migration velocity $\boldsymbol{v_m}$ normal to the interface [Humphreys and Hatherly, 2004]. However, this precludes local variations in chemical composition on the two sides of the interface. Furthermore, to a first approximation, the migration-rate modulus $v_m = |\boldsymbol{v_m}|$ is considered as a constant. This is clearly a strong limitation of the present model, since in many physical situations v_m varies both with position along the interface and with time. The latter case occurs in ″grain scale″ modeling of static or dynamic recrystallization, where the main driving force is the difference in average stored dislocation energy between the recrystallized grain and the matrix, which constitutes a simple extension of the model. Local changes of v_m may occur in turn, for instance due to the driving force component associated with interface curvature (capillarity effects). However, in such a case numerical calculation (finite difference or level set finite element method, phase field approach) should be involved.

To describe the current shape of the particle, it is necessary to derive the time (or strain) dependence of the spatial coordinates of any point *M* of the interface (Fig. 2). The displacement rate of the latter is given by the differential equation:

$$\frac{\mathrm{d}\boldsymbol{OM}}{\mathrm{d}\tau} = \boldsymbol{v_c} + \boldsymbol{v_m} \qquad (1)$$

where τ is the time. The direction of $\boldsymbol{v_m}$ involves the local shape of the interface, and Eq. (1) thus leads to quite complex partial derivative equations, which are difficult to solve, even numerically. It is possible, however, to use an indirect but smarter way, by considering the tangent line (*T*) at the current point *M* of the desired curve (or in 3D

the tangent plane (Π) at point M to the desired surface, see Appendix B). (T) is defined by the normal vector $\boldsymbol{OP}$ of modulus r and polar angle θ with initial values r_0 and θ_0 (P is referred to as the *podal point* associated with M). Under any uniform strain field, (T) remains a straight line. If one is able to derive the evolution of (T) with time τ, *i.e.* the two functions $r(\tau)$ and $\theta(\tau)$, the interface will be obtained as the envelope of the tangent lines for any given τ. This technique was applied successfully to the cases of uniaxial compression and simple shear, as will be described below. In the first one, the evolution of the axes can be separately derived due to symmetry considerations and will be addressed first. The shape of the particle is obtained in the form of two parametric equations $x = x(t, \varepsilon)$ and $z = z(t, \varepsilon)$, where $t = \tan\theta$ and ε is the axial strain (which identifies here to the von Mises equivalent strain) and both functions involve a non-analytic integral. By contrast, under simple shear the axes rotate during straining and their lengths and orientations cannot be determined analytically. The shape of the particle is derived again in a parametric form $x = x(t, \gamma)$ and $y = y(t, \gamma)$, where γ denotes the shear strain. It turns out that the two functions x and y are in this case fully analytical.

3. Uniaxial compression

It is sufficient to investigate the section of the interface by any plane (xz) containing the symmetry axis z. The advection velocity field is:

$$\boldsymbol{v_c} \begin{cases} \dot{\varepsilon} x/2 \\ -\dot{\varepsilon} z \end{cases} \tag{2}$$

where the axial strain rate $\dot{\varepsilon}\,(>0)$ identifies to the von Mises equivalent strain rate (*i.e.* $\dot{\varepsilon} = \dot{\bar{\varepsilon}} = -\dot{\varepsilon}_{zz}$ and therefore $\varepsilon = \bar{\varepsilon}$). The particle shape will obviously remain axisymmetric during combined advection and migration displacements. The length

changes of the axes can be analyzed first, before investigating the global shape of the particle.

3.1. Particle axes

If a and b are the lengths of the semiaxes parallel to z and x, respectively, Eq. (1) gives:

$$\begin{cases} \dfrac{\mathrm{d}a}{\mathrm{d}\tau} = -\dot{\varepsilon}a + v_m \quad \text{or} \quad \dfrac{\mathrm{d}a}{\mathrm{d}\varepsilon} = -a + \dfrac{v_m}{\dot{\varepsilon}} & \text{(3a)} \\ \dfrac{\mathrm{d}b}{\mathrm{d}\tau} = \dfrac{\dot{\varepsilon}b}{2} + v_m \quad \text{or} \quad \dfrac{\mathrm{d}b}{\mathrm{d}\varepsilon} = \dfrac{b}{2} + \dfrac{v_m}{\dot{\varepsilon}} & \text{(3b)} \end{cases}$$

Accounting for the fact that for $\tau = \varepsilon = 0$, $a = b = r_0$, integration of the above equations leads to:

$$\begin{cases} a = (r_0 - v_m/\dot{\varepsilon})\exp(-\varepsilon) + v_m/\dot{\varepsilon} & \text{(4a)} \\ b = (r_0 + 2v_m/\dot{\varepsilon})\exp(\varepsilon/2) - 2v_m/\dot{\varepsilon} & \text{(4b)} \end{cases}$$

(i) When $v_m > 0$ (particle growth), b increases monotonically with strain from its initial value r_0 to infinity. By contrast, since $\mathrm{d}a/\mathrm{d}\varepsilon = -(r_0 - v_m/\dot{\varepsilon})\exp(-\varepsilon)$, two different cases can occur: if $r_0 - v_m/\dot{\varepsilon} > 0$ or equivalently if $\alpha = v_m/r_0\dot{\varepsilon} < 1$, *a decreases* from r_0 to the asymptotic value $v_m/\dot{\varepsilon}$, whereas if $r_0 - v_m/\dot{\varepsilon} < 0$ or $\alpha > 1$, *a increases* from r_0 to $v_m/\dot{\varepsilon}$. In the particular case $\alpha = 1$, a remains constant during straining, which means that advection is exactly counterbalanced by migration. It is interesting to note that for any value of α the asymptotic shape of the particle is a disk of thickness $2v_m/\dot{\varepsilon}$ and infinite radius. In a similar way, the existence of an asymptotic thickness of grains under compression test has been reported previously [Gourdet and Montheillet, 2002] and it was shown that the migration rate of grain boundaries could be derived from the measurement of the average grain thickness after hot compression.

(ii) When $v_m < 0$ (particle dissolution), a decreases monotonically from r_0 to zero, which is attained for a critical strain ε_c^a given by $\exp(\varepsilon_c^a) = (r_0 - v_m/\dot{\varepsilon})/(-v_m/\dot{\varepsilon}) = (\alpha - 1)/\alpha$. Since $\mathrm{d}b/\mathrm{d}\varepsilon = (r_0/2 + v_m/\dot{\varepsilon})\exp(\varepsilon/2)$, two different cases can occur again: if $r_0/2 + v_m/\dot{\varepsilon} > 0$ or equivalently $\alpha > -1/2$, b *increases* from r_0 to infinity, while if $\alpha < -1/2$, b *decreases* from r_0 to zero which is attained for a critical strain ε_c^b such as $\exp(\varepsilon_c^b/2) = (v_m/\dot{\varepsilon})/(r_0/2 + v_m/\dot{\varepsilon}) = \alpha/(\alpha + 1/2)$. However, comparison of the two critical strains shows that $\varepsilon_c^a < \varepsilon_c^b$, and thus in the two cases the particle ends its life in the form of a disk of vanishing thickness for $\varepsilon = \varepsilon_c^a$. The final radius b_c can be determined by substituting ε_c^a for ε in Eq. (4b). In the special case $\alpha = -1/2$, it is easy to check that b remains equal to its initial value r_0 till the disappearance of the particle. The above discussion is summarized in Table 1.

Particles are usually characterized by their aspect ratio $\lambda = a/b$, which is here:

$$\lambda = \frac{r_0 \exp(-\varepsilon) + (v_m/\dot{\varepsilon})\left[1 - \exp(-\varepsilon)\right]}{r_0 \exp(\varepsilon/2) + 2(v_m/\dot{\varepsilon})\left[\exp(\varepsilon/2) - 1\right]} \tag{5}$$

Provided the initial radius r_0 is nonzero, Eq. (5) takes the form:

$$\lambda = \frac{\exp(-\varepsilon) + \alpha[1 - \exp(-\varepsilon)]}{\exp(\varepsilon/2) + 2\alpha[\exp(\varepsilon/2) - 1]} \tag{6}$$

which shows that the aspect ratio depends on the single parameter $\alpha = v_m/r_0\dot{\varepsilon}$. In the case $\alpha = 0$ (no migration), it is well known that the shape of the particle remains spheroidal during straining and Eq. (6) reduces to $\lambda = \exp(-3\varepsilon/2)$. A second special case occurs when $r_0 = 0$, which means that the particle nucleates at the onset of the deformation ($\varepsilon = 0$). Eq. (5) then gives:

$$\lambda = \frac{1-\exp(-\varepsilon)}{2\left[\exp(\varepsilon/2)-1\right]} \tag{7}$$

Quite surprisingly, the strain dependence of the aspect ratio is the same whatever the prescribed strain rate $\dot{\varepsilon}$ and the migration rate v_m. This point is discussed in greater detail in Appendix A. The strain dependence of λ in the various cases is shown in Fig. 3.

3.2. Analytical derivation of the particle shape

a) Equation of the tangent (*T*)

We start from the *normal equation* of the tangent (*T*) at a given time τ (or strain ε):

$$x\cos\theta + z\sin\theta = r \tag{8}$$

where the coefficients of *x* and *z* are the two components of the unit normal ***n*** to (*T*) (see Fig. 2). The first task is to derive the corresponding equation at time $\tau + \mathrm{d}\tau$ (or strain $\varepsilon + \dot{\varepsilon}\mathrm{d}\tau$). Migration does not change the slope of (*T*), *i.e.* the angle θ, but makes *r* change by $\mathrm{d}r = v_m \mathrm{d}\tau = (v_m/\dot{\varepsilon})\mathrm{d}\varepsilon$. To determine the effect of advection, the displacements of two points of (*T*), for instance the intersections *A* ($x_A = r/\cos\theta$) and *B* ($z_B = r/\sin\theta$) with the coordinate axes, are derived: these two points remain on the axes and their coordinates at time $\tau + \mathrm{d}\tau$ are given by x'_A and z'_B with $x'_A = x_A(1+\dot{\varepsilon}\mathrm{d}\tau/2) = x_A(1+\mathrm{d}\varepsilon/2)$ and $z'_B = z_B(1-\dot{\varepsilon}\mathrm{d}\tau) = z_B(1-\mathrm{d}\varepsilon)$. The equation of the tangent (*T*′) at time $\tau + \mathrm{d}\tau$ is then:

$$z'_B x + x'_A z = x'_A z'_B \tag{9}$$

This is still not the *normal* equation of (*T*′) that is obtained by dividing the two sides by $\sqrt{x'^2_A + z'^2_B}$. After some calculations, using a first order expansion with respect to $\mathrm{d}\varepsilon$, this leads to:

$$x\cos\theta\left(1-\frac{3}{2}\sin^2\theta\,\mathrm{d}\varepsilon\right)+z\sin\theta\left(1+\frac{3}{2}\cos^2\theta\,\mathrm{d}\varepsilon\right)=r\left(1-\frac{2\sin^2\theta-\cos^2\theta}{2}\mathrm{d}\varepsilon\right) \quad (10)$$

Alternatively, if dr and dθ are the increments of r and θ during the time increment dτ, the equation of (T') can also be written in the form:

$$x\cos(\theta+\mathrm{d}\theta)+y\sin(\theta+\mathrm{d}\theta)=r+\mathrm{d}r \quad (11)$$

or, to the first order in dr and dθ:

$$x(\cos\theta-\sin\theta\,\mathrm{d}\theta)+z(\sin\theta+\cos\theta\,\mathrm{d}\theta)=r+\mathrm{d}r \quad (12)$$

Identification of the coefficients of x and the right hand side term in Eqs (10) an (12) gives two first order differential equations for the functions r and θ of the variable ε, with initial conditions $r=r_0$ and $\theta=\theta_0$ for $\varepsilon=0$ (it is easy to check that identification of the coefficients of z is redundant):

$$\begin{cases} \dfrac{\mathrm{d}r}{\mathrm{d}\varepsilon}=\dfrac{r}{2}(\cos^2\theta-2\sin^2\theta)+\dfrac{v_m}{\dot{\varepsilon}} & (13a) \\ \dfrac{\mathrm{d}\theta}{\mathrm{d}\varepsilon}=\dfrac{3}{2}\sin\theta\cos\theta & (13b) \end{cases}$$

where the migration term $v_m/\dot{\varepsilon}$ has been incorporated in Eq. (13a).

Integration of Eq. (13b) is obvious and gives:

$$t=t_0\exp(3\varepsilon/2) \quad (14)$$

where $t=\tan\theta$ and $t_0=\tan\theta_0$. Substituting t for θ in Eq. (13a) then gives:

$$\frac{3t}{2}\frac{\mathrm{d}r}{\mathrm{d}t}-\frac{1-2t^2}{2(1+t^2)}r=\frac{v_m}{\dot{\varepsilon}} \quad (15)$$

Solving first the associated homogeneous equation leads to:

$$r^*=\frac{At^{1/3}}{\sqrt{1+t^2}} \quad (16)$$

Substituting then r^* for r in Eq. (15) and considering A as a function of t leads to $A=(2v_m/3\dot{\varepsilon})[K(t)+C]$, where C is a constant and $K(t)$ is an indefinite integral (non analytical) of the function $\sqrt{1+t^2}\,/\,t^{4/3}$. This gives:

$$r=\frac{2v_m}{3\dot{\varepsilon}}[K(t)+C]\frac{t^{1/3}}{\sqrt{1+t^2}} \tag{17}$$

Introducing the initial conditions and solving for r, we obtain:

$$r=\frac{t^{1/3}}{\sqrt{1+t^2}}\left[\frac{\sqrt{1+t_0{}^2}}{t_0{}^{1/3}}r_0+\frac{2}{3}\frac{v_m}{\dot{\varepsilon}}\Delta K(t_0,t)\right] \tag{18}$$

in which variables (ε,t) can be substituted for (t_0,t) using Eq. (14), leading to:

$$r=\frac{1}{\sqrt{1+t^2}}\left[\exp(\varepsilon/2)\sqrt{1+t^2\exp(-3\varepsilon)}\,r_0+\frac{2}{3}t^{1/3}\Delta K\left[t\exp(-3\varepsilon/2),t\right]\frac{v_m}{\dot{\varepsilon}}\right] \tag{19}$$

In the last two equations, the definite integral $\Delta K(t_0,t)=K(t)-K(t_0)$, *i.e.*:

$$\Delta K(t_0,t)=\Delta K\left[t\exp(-3\varepsilon/2),t\right]=\int_{t\exp(-3\varepsilon/2)}^{t}\frac{\sqrt{1+u^2}}{u^{4/3}}du=\Delta K(\varepsilon,t) \tag{20}$$

was introduced. Eq. (19) specifies the position of the tangent (*T*) in the (*xz*) plane for any polar angle θ at a strain ε. The associated Cartesian equation is given by Eq. (8), noting that $\cos\theta=1/\sqrt{1+t^2}$ and $\sin\theta=t/\sqrt{1+t^2}$:

$$x+tz=\exp(\varepsilon/2)\sqrt{1+t^2\exp(-3\varepsilon)}\,r_0+\frac{2}{3}t^{1/3}\Delta K\left[t\exp(-3\varepsilon/2),t\right]\frac{v_m}{\dot{\varepsilon}} \tag{21}$$

b) Equation of the envelope

The last task is to find the envelope of the tangents (*T*) when *t* varies, for any given strain ε. This is achieved by taking the derivatives of the two sides of Eq. (21) with respect to *t* and solving for *x* and *z* [see, *e.g.*, *Wikipedia*, 2018]. We thus get:

$$\begin{cases} x = \dfrac{\exp(\varepsilon/2)}{\sqrt{1+t^2\exp(-3\varepsilon)}} r_0 + \dfrac{2}{3}\left[\dfrac{2}{3}t^{1/3}\Delta K(\varepsilon,t) - t^{4/3}\partial_t \Delta K(\varepsilon,t)\right]\dfrac{v_m}{\dot{\varepsilon}} & \text{(22a)} \\ z = \dfrac{t\exp(-5\varepsilon/2)}{\sqrt{1+t^2\exp(-3\varepsilon)}} r_0 + \dfrac{2}{3}\left[\dfrac{1}{3}t^{-2/3}\Delta K(\varepsilon,t) + t^{1/3}\partial_t \Delta K(\varepsilon,t)\right]\dfrac{v_m}{\dot{\varepsilon}} & \text{(22b)} \end{cases}$$

where $\Delta K(\varepsilon,t)$ is given by Eq. (20), from which the partial derivative $\partial_t \Delta K(\varepsilon,t)$ with respect to t is readily calculated:

$$\partial_t \Delta K(\varepsilon,t) = \left[\frac{\partial \Delta K(\varepsilon,t)}{\partial t}\right]_\varepsilon = \frac{\sqrt{1+t^2}}{t^{4/3}} - \frac{\sqrt{1+t^2\exp(-3\varepsilon)}}{t^{4/3}}\exp(\varepsilon/2) \qquad \text{(22c)}$$

With θ varying from $-\pi/2$ to $+\pi/2$, Eqs (22a) and (22b) give a parametric representation of the matrix-particle interface in (xz) plane, for any given strain ε. It is worth to note that:

(i) When $v_m = 0$ (pure advection), Eqs (22a) and (22b) lead to:

$$\frac{x^2}{{r_0}^2\exp(\varepsilon)} + \frac{z^2}{{r_0}^2\exp(-2\varepsilon)} = 1 \qquad \text{(23)}$$

which is the equation of an ellipse of semiaxes $r_0\exp(\varepsilon/2)$ and $r_0\exp(-\varepsilon)$ parallel to x and z, respectively, as expected.

(ii) If r_0 is taken as unit length, the only parameter is $\alpha = v_m/r_0\dot{\varepsilon}$. Furthermore, if $r_0 = 0$, to the scaling factor $v_m/\dot{\varepsilon}$, the shape of the growing particle depends only on the applied strain ε, whatever v_m and $\dot{\varepsilon}$ (see Appendix A).

3.3. Shape changes of particles under uniaxial compression

The above results are illustrated in Fig. 4 for an initially spherical particle of radius $r_0 = 1$ or 0 and axial strains ranging from 0 to 1: In the absence of boundary migration (Fig. 4a), the particle becomes merely a spheroid according to Eq. (23). Fig. 4b shows

the case of a particle *growing* during deformation. Although penny shaped, it is *not* a spheroid. In the present case, $r_0 = 0.8$ and $v_m/\dot{\varepsilon} = 1$, $\alpha > 1$, which means that *a* increases up to the asymptotic value 1, while *b* tends to infinity. The special case $r_0 = 0$, which corresponds to the nucleation and subsequent growth of a particle during straining, is shown in Fig. 4c, where it looks even more "rounded" (see the aspect ratio in Fig. 3). In Fig. 4d, $v_m/\dot{\varepsilon} = -1$ which means that the particle *shrinks* during straining (dissolution). Since $\alpha = -0.56 < -1/2$, it takes the form of a disk of decreasing thickness, which would eventually vanish at $\varepsilon_c^a = 1.03$ (see section 3.1) . However, the present analytical calculations are no longer valid at large strains since a cusp appears at $z = 0$ for a strain close to 0.8 as shown by the figure. More quantitative results can be derived, such as the strain dependence of the particle volume for various values of $v_m/\dot{\varepsilon}$ (Fig. 5a). Since the shape is not ellipsoidal, the volume was calculated numerically (see Appendix C). However, the figure shows that a very close approximation is obtained by taking the volume $V_{app} = (4/3)\pi a^2 b$ of the spheroid of semiaxes *a* and *b*. In the same way, the surface area changes of the particle are depicted in Fig. 5b. An analytical approximation is proposed as the surface of the *oblate* spheroid ($\lambda < 1$) of semiaxes *a* and *b* [Eqs (4a) and (4b)], *i.e.*:

$$S_{app=}\, 2\pi\left[b^2 + \frac{a^2 b}{c}\ln\left(\frac{b+c}{a}\right)\right] \tag{24}$$

where $c = \sqrt{b^2 - a^2}$. As expected, the surface area increases in the absence of boundary migration ($v_m = 0$).

4. Simple shear

4.1. Analytical derivation of the particle shape

The simple shear case is more complex, since the evolution of the particle is fully three-dimensional as soon as the migration rate v_m is not zero. If (xz) and x are the shear plane and shear direction, respectively, it is nevertheless sufficient to analyze the section of the interface by the plane of symmetry (xy) to form an adequate mental picture of the particle. The analysis below is thus restricted to the (xy) plane which contains the two terms $\boldsymbol{v_c}$ and $\boldsymbol{v_m}$ of the displacement rate, while its 3-D extension is reported in Appendix B. Moreover, the analysis is made more difficult than in uniaxial compression because the axes of the particle (which incidentally are not derived in closed form) rotate during deformation. The simple shear advection velocity field is now:

$$\boldsymbol{v_c} \begin{cases} \dot{\gamma} y \\ 0 \end{cases} \tag{25}$$

where $\dot{\gamma}\,(>0)$ is the shear strain rate. The latter is related to the von Mises equivalent strain rate by the equation $\dot{\bar{\varepsilon}} = \dot{\gamma}/\sqrt{3}$ and, as a corollary, the equivalent von Mises strain is $\bar{\varepsilon} = \gamma/\sqrt{3}$ where γ is the shear strain. The same method as in Section 3.2 is used to derive the evolution of a tangent to the desired interface, which leads to the following two differential equations:

$$\begin{cases} \dfrac{\mathrm{d}r}{\mathrm{d}\gamma} = r\sin\theta\cos\theta + \dfrac{v_m}{\dot{\gamma}} & \text{(26a)} \\ \dfrac{\mathrm{d}\theta}{\mathrm{d}\gamma} = -\cos^2\theta & \text{(26b)} \end{cases}$$

Integration of Eq. (26b) readily gives:

$$t = t_0 - \gamma \tag{27}$$

where $t = \tan\theta$ and $t_0 = \tan\theta_0$. Substituting t for θ in Eq. (26a) then gives after integration:

$$r = \frac{\sqrt{1+(t+\gamma)^2}}{\sqrt{1+t^2}} r_0 + \left[\frac{(t+\gamma)\sqrt{1+(t+\gamma)^2} - t\sqrt{1+t^2} + \sinh^{-1}(t+\gamma) - \sinh^{-1}(t)}{\sqrt{1+t^2}} \right] \frac{v_m}{2\dot{\gamma}} \qquad (28)$$

This gives the equation of the tangent:

$$x + ty = \sqrt{1+(t+\gamma)^2}\, r_0 + \left[(t+\gamma)\sqrt{1+(t+\gamma)^2} - t\sqrt{1+t^2} + \sinh^{-1}(t+\gamma) - \sinh^{-1}(t) \right] \frac{v_m}{2\dot{\gamma}} \qquad (29)$$

Taking then the derivatives of the two sides of Eq. (29) with respect to t and solving for x and y gives parametric equations for the particle surface in the symmetry plane (xy):

$$\begin{cases} x = \dfrac{1+\gamma(t+\gamma)}{\sqrt{1+(t+\gamma)^2}} r_0 + \left[(\gamma - t)\sqrt{1+(t+\gamma)^2} + t\sqrt{1+t^2} + \sinh^{-1}(t+\gamma) - \sinh^{-1}(t) \right] \dfrac{v_m}{2\dot{\gamma}} & (30a) \\ y = \dfrac{t+\gamma}{\sqrt{1+(t+\gamma)^2}} r_0 + 2\left[\sqrt{1+(t+\gamma)^2} - \sqrt{1+t^2} \right] \dfrac{v_m}{2\dot{\gamma}} & (30b) \end{cases}$$

The full three-dimensional equations of the surface are given in Appendix B.

4.2. Shape changes of particles under simple shear

The above results are illustrated in Figs 6a,b,c for an initially spherical growing particle of radius $r_0 = 1$ or 0 and equivalent strains ranging from 0 to 1 (*i.e.* $0 \le \gamma \le 1.732$): In the absence of boundary migration (Fig. 6a), it is easy to check that Eqs (30a) and (30b) with $v_m = 0$ reduce to the Cartesian equation of an ellipse:

$$x^2 + (1+\gamma^2)y^2 - 2\gamma xy = {r_0}^2 \qquad (31)$$

The major and minor axes make angles α_{max} and α_{min} with the x-axis and their lengths are:

$$a_{max} = \sqrt{2} r_0 \Big/ \left[\gamma^2 + 2 - \gamma \sqrt{\gamma^2 + 4} \right]^{1/2} \qquad (32a)$$

and:

$$a_{min} = \sqrt{2} r_0 \Big/ \left[\gamma^2 + 2 + \gamma \sqrt{\gamma^2 + 4} \right]^{1/2} \qquad (32b)$$

The third axis of the ellipsoid is parallel to z and, since simple shear is a plane strain deformation, its length $c = 1$ remains constant.

Fig. 6b shows the case of a growing particle. Sections by the (xy) plane look roughly like ellipses, although they are not. When $r_0 = 0$ (Fig. 6c), it becomes more obvious that the sections are more "rounded" than ellipses. Moreover, it is interesting to note that, in the same way as in uniaxial compression, the ratio $v_m / \dot{\gamma}$ appears merely as a scaling factor, which means that the shape of the particle depends only on the strain γ, whatever the shear strain rate $\dot{\gamma}$ and the migration rate v_m (see Appendix A). In the case of a shrinking particle (Fig. 6d), a cusp appears at the end of the major axis for a strain close to 0.5 as shown by the figure, and the calculations are no longer valid at larger strains. It is still possible to define two main axes in the (xy) plane, for example the maximum a_{max} and minimum a_{min} radii of the curve, which were determined numerically. The aspect ratios $\lambda = a_{min} / a_{max}$ are reported in Fig. 3; this diagram shows that, when plotted as a function of the *equivalent strain*, the evolutions of λ in uniaxial compression and simple shear are very similar. In both cases, the particle is clearly less flattened when it grows and conversely more flattened during shrinking. The angle of the particle major axis to the x-axis is shown in turn as a function of the shear strain γ in Fig. 7. By contrast to λ, the latter is not strongly modified by grain boundary migration. Nevertheless, it appears clearly that the rotation rate of the major axis towards the x-axis becomes faster when the particle shrinks, while it is decelerated for

a growing particle.

In all cases the two opposite points with horizontal tangent are associated with $\theta = \pm \pi/2$ or $t \to \pm \infty$. For $\theta = \pi/2$ (*e.g.* point *P* in Fig. 8), Eqs (32a) and (32b) give quite simple expressions of the coordinates ξ and η of *P*, after evaluation of some indeterminate forms:

$$\begin{cases} \xi = \gamma r_0 + \dfrac{\gamma^2}{2} \dfrac{v_m}{\dot{\gamma}} \\ \eta = r_0 + \gamma \dfrac{v_m}{\dot{\gamma}} \end{cases} \tag{33}$$

This observation strongly suggests to consider the ellipse (*E*), centered in *O* with horizontal tangent in *P,* as an approximation to the particle shape. The latter is simply obtained from the circle of radius η by a simple shear of amplitude $\bar{\gamma} = \xi/\eta$, as shown in Fig. 8. The equation of (*E*) as well as the lengths of its axes are then given by substituting $\bar{\gamma}$ for γ in Eqs (31) and (32a, b). Figs 8a and b illustrate this fit for the two cases of particle growth and dissolution, respectively.

Finally, the computed volumes and surfaces of the particle are displayed in Figs 9a and b as a function of the shear strain γ (see Appendix C). It appears that the volume is perfectly well estimated by the analytical volume of the respective approximate ellipsoid. (Note that the latter is merely equal to the volume of the sphere of radius η).

Finally, a significant parameter is the surface to volume ratio S/V of the particle. It is important to take into account, since in the present approach as well as in a number of models of grain growth or recrystallization, surface energy is neglected to a first approximation. Fig. 10a shows that for a particle of nonzero initial volume, S/V remains almost constant or decreases slightly during uniaxial compression or simple shear loading for pure advection or particle growth. By contrast, it increases strongly

when the particle in shrinking, which means that surface energy should be involved in such a case. That is even more true for the growth of a particle of zero initial radius (Fig. 10b).

5. Conclusions

The conclusions of the present investigation are first to be drawn in terms of methodology: it was shown that the evolution of the interface between a growing or shrinking (dissolving) particle and the surrounding deforming matrix can be determined as the envelope of a family of straight lines or planes. In the simple cases of uniaxial compression and simple shear, and assuming constant (in space and time) normal migration rate of the boundary, results have been given in a completely analytical form.

The main outcomes of the calculations are the following:

(a) It was shown that for a particle growing from a zero initial radius, the ratio between the migration rate and the applied strain rate acts merely as a scaling factor. In consequence, quite surprisingly, the aspect ratio of the particle is independent of the above two parameters.

(b) The shapes of the deforming particles are not, although they are always close to, ellipsoids whenever the migration rate of the boundary is not zero. Therefore, they can be fitted by ellipsoids which have been derived analytically.

(c) The strain dependence of the aspect ratios is very similar for the two types of loading, provided the von Mises equivalent strain is used. In both cases, particle flattening or elongation is reduced by growth, and conversely increased by shrinking (dissolution).

(d) In simple shear, the rotation of the particle main axes is only weakly dependent of

the loading conditions, even with an initial zero radius.

Further works can be suggested using less restrictive conditions, including more complex strain paths (*e.g.*, combination of compression and plane shear) or migration rate changing in time and / or in space. For instance, an application of the approach to the grain shape evolution during dynamic recrystallization, involving successive growth and shrinking, could be carried out straightforwardly from the present results. Moreover, a natural extension of the model would be to include the driving force component due to interface curvature, that would require the use of numerical calculation (e.g., finite difference or finite element method, phase field approach).

Appendix A

Shape change of a particle of zero initial radius

It has been shown that the evolution of an initially spherical particle under both uniaxial compression and simple shear, with constant boundary-migration rate v_m, was governed by a differential equation of the form:

$$\frac{\mathrm{d}r}{\mathrm{d}\varepsilon} - r f_1(\theta) = \frac{v_m}{\dot{\varepsilon}} \tag{A.1}$$

where r and θ are the current coordinates of the podal point P of the desired interface (in simple shear, γ stands for ε). More specifically, for uniaxial compression [Eq. (13a)]:

$$f_1(\theta) = \frac{1}{2}(\cos^2\theta - 2\sin^2\theta) \tag{A.2}$$

and for simple shear [Eq. (26a)]:

$$g_1(\theta) = \sin\theta\cos\theta \tag{A.3}$$

In the above equations, it is possible to replace θ (Eulerian standpoint) by θ_0 and ε or γ (Lagrangian standpoint), where θ_0 is the value of θ at $\varepsilon = 0$ [see Eqs (14) and (27)], which yields:

$$f_2(t_0,\varepsilon) = \frac{1 - 2{t_0}^2\exp(3\varepsilon)}{2[1 + {t_0}^2\exp(3\varepsilon)]} \tag{A.4}$$

$$g_2(t_0,\varepsilon) = \frac{t_0 - \gamma}{1 + (t_0 - \gamma)^2} \tag{A.5}$$

We assume now that the radial coordinate of the podal point fulfils a slightly more general differential equation, allowing the migration rate to depend on θ_0 and ε:

$$\frac{\mathrm{d}r}{\mathrm{d}\varepsilon} - r f(\theta_0,\varepsilon) = \frac{v_m}{\dot{\varepsilon}} h(\theta_0,\varepsilon) \tag{A.6}$$

Integrating first the associated homogeneous equation with respect to ε for any given θ_0 gives:

$$\ln\left(\frac{r^*}{A}\right) = \int f(\theta_0, \varepsilon)\mathrm{d}\varepsilon = F(\theta_0, \varepsilon) \tag{A.7}$$

where A is an integration constant. Then:

$$r^* = A\exp[\mathrm{F}(\theta_0, \varepsilon)] \tag{A.8}$$

Substituting then r^* for r in Eq. (A.6) and considering A as a function of ε leads to:

$$\frac{\mathrm{d}A}{\mathrm{d}\varepsilon} = \frac{v_m}{\dot{\varepsilon}} h(\theta_0, \varepsilon)\exp[-F(\theta_0, \varepsilon)] \tag{A.9}$$

whence:

$$A = \frac{v_m}{\dot{\varepsilon}}\left[\int h(\theta_0, \varepsilon)\exp[-F(\theta_0, \varepsilon)]\mathrm{d}\varepsilon + C\right] \tag{A.10}$$

or:

$$A = \frac{v_m}{\dot{\varepsilon}}[J(\theta_0, \varepsilon) + C] \tag{A.11}$$

and therefore:

$$r = \frac{v_m}{\dot{\varepsilon}}[J(\theta_0, \varepsilon) + C]\exp[\mathrm{F}(\theta_0, \varepsilon)] \tag{A.12}$$

The constant C is such that $r = r_0$ for $\varepsilon = 0$, which gives:

$$r_0 = \frac{v_m}{\dot{\varepsilon}}[J(\theta_0, 0) + C]\exp[\mathrm{F}(\theta_0, 0)] \tag{A.13}$$

Finally, combination of the last two equations yields:

$$r = \left\{\frac{r_0}{\exp[\mathrm{F}(\theta_0, 0)]} + \frac{v_m}{\dot{\varepsilon}}[J(\theta_0, \varepsilon) - J(\theta_0, 0)]\right\}\exp[F(\theta_0, \varepsilon)] \tag{A.14}$$

In the case where the initial radius of the particle is zero, $v_m/\dot{\varepsilon}$ stands merely as a scaling factor of r. In particular, for any given strain ε the ratio of the minimum and

maximum r, *i.e.* the aspect ratio of the particle, is independent of both the prescribed strain rate and the migration rate of the interface.

Appendix B

Three-dimensional analysis of the simple shear case

The tangent plane (Π) at point M to the desired surface is now considered (Fig. B.1). (Π) is defined by the normal vector $\boldsymbol{OP}$ of modulus r and polar angles θ and φ with initial values r_0, θ_0, and φ_0 (P is the podal point associated with M). Under any uniform strain field, (Π) remains a plane. If one is able to derive the evolution of (Π) with time τ, *i.e.* the three functions $r(\tau)$, $\theta(\tau)$, and $\varphi(\tau)$, the interface will be obtained as the envelope of the tangent planes for any given τ. Since the normal unit of $\boldsymbol{OP}$ is $\boldsymbol{n}(\cos\theta\cos\varphi, \sin\theta, \cos\theta\sin\varphi)$, the normal equation of plane (Π) is:

$$x\cos\theta\cos\varphi + y\sin\theta + z\cos\theta\sin\varphi = r \tag{B.1}$$

After derivation of the corresponding equation at time $\tau + \mathrm{d}\tau$ (or shear strain $\gamma + \dot{\gamma}\mathrm{d}\tau$), and following the same way as in Section 3.2, three first order differential equations for the functions r, θ, and φ of the variable γ are obtained:

$$\begin{cases} \dfrac{\mathrm{d}r}{\mathrm{d}\gamma} = r\sin\theta\cos\theta\cos\varphi + \dfrac{v_m}{\dot{\gamma}} & \text{(B.2a)} \\ \dfrac{\mathrm{d}\theta}{\mathrm{d}\gamma} = -\cos^2\theta\cos\varphi & \text{(B.2b)} \\ \dfrac{\mathrm{d}\varphi}{\mathrm{d}\gamma} = 0 & \text{(B.2c)} \end{cases}$$

which first leads to the first conclusion that the podal point P stays in a fixed plane $\varphi = \varphi_0$ during straining. (Note that this does not hold for the current point M of the

interface). Equations (B.2a) and (B.2b) can then be written:

$$\begin{cases} \dfrac{\mathrm{d}r}{\cos\varphi_0\,\mathrm{d}\gamma} = r\sin\theta\cos\theta + \dfrac{v_m}{\dot{\gamma}\cos\varphi_0} & \text{(B.3a)} \\ \dfrac{\mathrm{d}\theta}{\cos\varphi_0\,\mathrm{d}\gamma} = -\cos^2\theta & \text{(B.3b)} \end{cases}$$

This system of equations is formally identical to Eqs (26a) and (26b) provided that $\gamma\cos\varphi_0$ is substituted for γ. In particular, this leads to:

$$t = t_0 - \gamma\cos\varphi_0 \qquad \text{(B.4)}$$

where $t = \tan\theta$ and $t_0 = \tan\theta_0$, and Eq. (B.1) can be written:

$$x\cos\varphi + ty + z\sin\varphi = \rho \qquad \text{(B.5)}$$

where $\rho = r\sqrt{1+t^2}$. This equation represents a family of planes (Π) depending on two independent parameters $\varphi\,(=\varphi_0)$ and t (Eulerian standpoint) or φ_0 and t_0 (Lagrangian standpoint). Its envelope is determined by taking the partial derivatives of the two sides with respect to t and φ and solving the following system for x, y, and z:

$$\begin{cases} x\cos\varphi + ty + z\sin\varphi = \rho & \text{(B.5)} \\ y = \partial\rho/\partial t & \text{(B.6a)} \\ -x\sin\varphi + z\cos\varphi = \partial\rho/\partial\varphi & \text{(B.6b)} \end{cases}$$

This yields:

$$\begin{cases} x = \left(\rho - t\dfrac{\partial\rho}{\partial t}\right)\cos\varphi - \dfrac{\partial\rho}{\partial\varphi}\sin\varphi & \text{(B.7a)} \\ y = \partial\rho/\partial t & \text{(B.6a)} \\ z = \left(\rho - t\dfrac{\partial\rho}{\partial t}\right)\sin\varphi + \dfrac{\partial\rho}{\partial\varphi}\cos\varphi & \text{(B.7b)} \end{cases}$$

After some simple but somewhat tedious calculations, fully explicit expressions are

found for x, y, and z:

$$\begin{cases} x = \dfrac{\cos\varphi + \gamma(t + \gamma\cos\varphi)}{\sqrt{1 + (t + \gamma\cos\varphi)^2}} r_0 \\ + \left\{ (1 - \tan^2\varphi)\left[\sinh^{-1}(t + \gamma\cos\varphi) - \sinh^{-1}(t) \right] - (1 + \tan^2\varphi)\left[(t - \gamma\cos\varphi)\sqrt{1 + (t + \gamma\cos\varphi)^2} - t\sqrt{1 + t^2} \right] \right\} \dfrac{v_m}{2\dot{\gamma}} \end{cases} \tag{B.8a}$$

$$y = \frac{t + \gamma\cos\varphi}{\sqrt{1 + (t + \gamma\cos\varphi)^2}} r_0 + 2\left[\frac{\sqrt{1 + (t + \gamma\cos\varphi)^2} - \sqrt{1 + t^2}}{\cos\varphi} \right] \frac{v_m}{2\dot{\gamma}} \tag{B.8b}$$

$$z = \frac{\sin\varphi}{\sqrt{1 + (t + \gamma\cos\varphi)^2}} r_0 + 2\left[\sinh^{-1}(t + \gamma\cos\varphi) - \sinh^{-1}(t) \right] \tan\varphi \frac{v_m}{2\dot{\gamma}} \tag{B.8c}$$

The above three equations, with θ varying from $-\pi/2$ to $+\pi/2$ and φ from 0 to π, are a parametric representation of the three-dimensional surface of the particle.

Appendix C

Numerical calculation procedures

Two *Python* scripts were developed: the first one computes the evolution of the particle shape and size for increasing shear strains after discretizing the t variable in Eqs (30a) and (30b). A special care was devoted to the case where the particle collapses. The second *Python* script computes the time evolution in a Lagrangian formulation of the 3D particle in shear strain according to the equations given in Appendix B. Each point M of a particle surface has the following expression in a spherical coordinate system:

$$\boldsymbol{OM} = x(\theta,\varphi)\,\boldsymbol{i} + y(\theta,\varphi)\,\boldsymbol{j} + z(\theta,\varphi)\,\boldsymbol{k} \tag{C.1}$$

The shape is computed for each shear strain. The area A and volume V of the particle are given respectively by the integrals:

$$A = \iint_S \left\| \frac{\partial \boldsymbol{OM}}{\partial \theta} \times \frac{\partial \boldsymbol{OM}}{\partial \varphi} \right\| \mathrm{d}\theta \, \mathrm{d}\varphi \tag{C.2}$$

and

$$V = \iint_S z \left(\frac{\partial x}{\partial \theta} \frac{\partial y}{\partial \varphi} - \frac{\partial y}{\partial \theta} \frac{\partial x}{\partial \varphi} \right) d\theta \, d\varphi \tag{C.3}$$

It is worth to mention that the determination of A and V requires the computation of six partial derivatives, which is efficiently carried out thanks to *SymPy*, a *Python* library for symbolic mathematics. These two surface integrals are numerically evaluated thanks to the 2D trapezoidal rule. For each value of the shear strain, the two *Python* scripts generate a set of .vtk files for easy post-processing and 3D visualization thanks to *Paraview's* software.

Acknowledgements. One of the authors (FM) is indebted to Dr. G. Damamme (French Atomic Energy Commission) for his essential suggestions and fruitful discussions about the analytical calculation procedure.

Table and figure captions

Table 1. Evolution with prescribed axial strain of the minor (a) and major (b) semiaxes of a particle for a negative (dissolution), zero, or positive (growth) migration rate v_m. The asymptotic shape of the particle is also indicated.

Figure 1. (a) Two-dimensional simulation of grain growth using a *vertex* model: grain boundary movement with respect to matter (*migration*) [Maurice and Humphreys, 1998]; (b) Schematic representation of grain boundary movement driven by matter

(*advection*) in the case of plane strain compression [*after* Maurice and Humphreys, 1998].

Figure 2. Illustration of the tangent (*T*) at point *M* to the particle-matrix interface. Vector ***OP*** defined by its polar coordinates *r* and θ is normal to (*T*) and *P* is the podal point associated with *M*.

Figure 3. Equivalent strain dependence of the particle aspect ratio in uniaxial compression (analytical results, solid lines) and simple shear (numerical results, broken lines). For $r_0 = 0$, the evolution is independent of $v_m/\dot{\bar{\varepsilon}}$; for $r_0 = 1$, three values of $v_m/\dot{\bar{\varepsilon}}$ are compared.

Figure 4. Axial sections showing the evolution of the particle shape in uniaxial compression for axial strains ranging from 0 to 1; (a) $v_m/\dot{\varepsilon} = 0$, pure advection effect; (b) Case of a particle growing towards an asymptotic platelet shape (see Table 1); (c) Special case where $r_0 = 0$: the particle shape is independent of $v_m/\dot{\varepsilon}$, which acts merely as a scaling factor; (d) Case of a shrinking particle (for strains larger than 0.8, the calculation is no longer valid).

Figure 5. (a) Strain dependence of the particle volume (solid lines) in uniaxial compression: For $r_0 = 0$, $v_m/\dot{\varepsilon}$ acts merely as a scaling factor; for $r_0 = 1$, three values of $v_m/\dot{\varepsilon}$ are compared, corresponding to particle growth, pure advection (constant volume), and particle shrinking, respectively. The volumes of the associated spheroids of semiaxes *a* and *b* are also shown (crosses). (b) Strain dependence of the particle

surface area (solid lines) in uniaxial compression in the same cases as illustrated in Fig. 5a; The surfaces of the associated spheroids of semiaxes *a* and *b* are also shown (crosses).

Figure 6. Sections by the plane of symmetry (*xy*) showing the evolution of the particle shape in simple shear for equivalent strains ranging from 0 to 1 (*i.e.* shear strains from 0 to $\sqrt{3}=1.732$); (a) $v_m/\dot{\bar{\varepsilon}}=0$, pure advection effect; (b) Case of a growing particle; (c) Special case where $r_0=0$: the particle shape is independent of $v_m/\dot{\bar{\varepsilon}}$, which acts merely as a scaling factor; (d) Case of a shrinking particle (beyond a strain of 0.5, the calculation is no longer valid).

Figure 7. Shear strain dependence of the particle major axis to the *x*-axis. For $r_0=0$, the evolution is independent of $v_m/\dot{\gamma}$. For $r_0=1$, three values of $v_m/\dot{\gamma}$ are compared, corresponding to particle growth, pure advection, and particle shrinking, respectively. Results pertaining to the elliptical approximation are also shown (crosses).

Figure 8. Approximation of the particle section in the (*xy*) plane by an ellipse in simple shear (broken lines). The ellipse is obtained from the circle of radius η by a simple shear of amplitude $\bar{\gamma}=\xi/\eta$ (see text). The initial particle shape (circle of radius $r_0=1$) is also shown; (a) particle growth; (b) particle shrinking.

Figure 9. (a) Shear strain dependence of the particle volume in simple shear. For $r_0=0$, $v_m/\dot{\gamma}$ acts merely as a scaling factor; note that the volume growth is very weak. For $r_0=1$, three values of $v_m/\dot{\gamma}$ are compared, corresponding to particle growth, pure

advection (constant volume), and particle shrinking, respectively. Results obtained from the elliptical approximation are also shown (crosses). (b) Shear Strain dependence of the particle surface in simple shear in the same cases as illustrated in Fig. 9a.

Figure 10. (a) Equivalent strain dependence of the surface to volume ratio of a particle of initial radius $r_0 = 1$ for uniaxial compression (solid lines) and simple shear loading (broken lines). Three values of $v_m / \dot{\bar{\varepsilon}}$ are compared, corresponding to particle growth, pure advection, and particle shrinking, respectively. (b) Case of a growing particle with initial radius $r_0 = 0$ ($v_m / \dot{\bar{\varepsilon}} = 0.5$).

Figure B.1. Illustration of the tangent plane (Π) at point M to the desired surface. (Π) intersects the three coordinate axes at points A, B, and C. Vector ***OP*** defined by its polar coordinates r, θ, and φ is normal to (Π).

List of references

Bernacki M., Resk H., Coupez T., Logé R.E., Finite element model of primary recrystallization in polycrystalline aggregates using a level set framework, Modelling Simul. Mater. Sci. Eng. 17 (2009) 064006.
https://doi:10.1088/0965-0393/17/6/064006

Budianski B., Hutchinson J.W., Slutsky S., Void growth and collapse in viscous solids, The R. Hill 60th Anniversary volume, eds. Hopkins H.G. et Sewell M.J., Pergamon Press, Oxford, 1982, pp. 13-44.

Burke J., Turnbull D., Recrystallization and grain growth. Prog. Met. Phys. 3 (1952) 220–292.

Duddu R., Chopp D.L., Voorhees P., Moran B., Diffusional evolution of precipitates in elastic media using the extended finite element and the level set methods, J. Comput. Phys. 230 (2011) 1249-1264.
https://doi:10.1016/j.jcp.2010.11.002

Gilormini P., Montheillet F., Deformation of an inclusion in a viscous matrix and induced stress concentrations, J. Mech. Phys. Solids 34 (1986) 97-123.

Gourdet S., Montheillet F., Effects of dynamic grain boundary migration during the hot compression of high stacking fault energy metals, Acta Mater. 50 (2002) 2801-2812.

Hesselbarth H.W., Göbel I.R., Simulation of recrystallization by cellular automata, Acta Metall. Mater. 39 (1991) 2135-2143.

Humphreys F.J., Hatherly M., Recrystallization and related annealing phenomena, 2nd edn., Elsevier, Oxford (2004).
https://doi.org/10.1016/C2009-0-07986-0

Maire L., Fausty J., Bernacki M., Bozzolo N., De Micheli P., Moussa C., A new topological approach for the mean field modeling of dynamic recrystallization, Mater. Des. 146 (2018) 194-207.
https://doi.org/10.1016/j.matdes.2018.03.011

Maire L., Scholtes B., Moussa C., Bozzolo N., Pino Muñoz D., Settefrati A., Bernacki M., Modeling of dynamic and post-dynamic recrystallization by coupling a full field approach to phenomenological laws, Mater. Des. 133 (2017) 498-519. http://dx.doi.org/10.1016/j.matdes.2017.08.015

Maurice C., Humphreys F.J., 2- and 3-D curvature driven vertex simulations of grain growth, in: H. Weiland (Ed.), Grain growth in polycrystalline materials III, The Minerals, Metals and Materials Society, Warrendale PA, 1998, pp. 81-90.
ISBN : 0873394097

Moelans N., Godfrey A., Zhang Y.B., Juul Jensen D., Phase-field simulation study of the migration of recrystallization boundaries, Phys. Rev. B, 88 (2013) 054103. https://doi.org/10.1103/PhysRevB.88.054103

Montheillet F., Piot D., Combined effects of grain boundary convection and migration in dynamic phase transformations. Thermec-2016, Graz, Autriche (2016), in: Materials Science Forum, 879 (2017) 72-77.
http://doi:10.4028/www.scientific.net/MSF.879.72.

Piot D., Smagghe G., Jonas J.J., Desrayaud C., Montheillet F., Perrin G., Montouchet A., Kermouche G., A semitopological mean-field model of discontinuous dynamic recrystallization, J. Mater. Sci. 53 (2018) 8554-8566.
https://doi.org/10.1007/s10853-018-2137-3

Ruiz Sarrazola D.A., Maire L., Moussa C., Bozzolo N., Pino Muñoz, D., Bernacki M., Full field modeling of dynamic recrystallization in a CPFEM context – Application to 304L steel, Comput. Mater. Sci. 184 (2020) 109892.
https://doi.org/10.1016/j.commatsci.2020.109892

Ruiz Sarrazola D.A., Pino Muñoz D., Bernacki M., A new numerical framework for the full field modeling of dynamic recrystallization in a CPFEM context, Comput. Mater. Sci. 179 (2020) 109645.
https://doi.org/10.1016/j.commatsci.2020.109645

Wikipedia (2018), Envelope (mathematics)
https://en.wikipedia.org/wiki/Envelope_(mathematics)

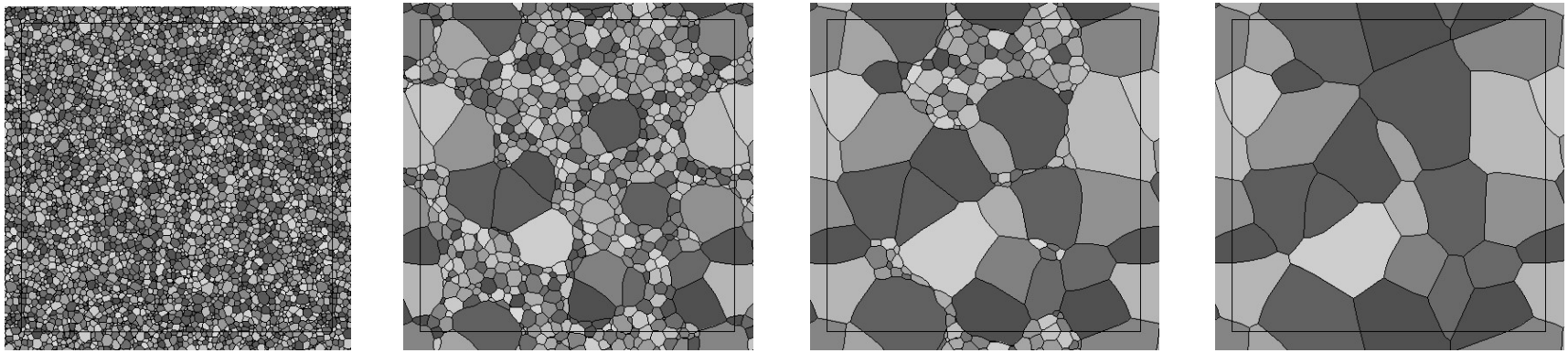

[Maurice & Humphreys, 1998]

(a)

Figure 1

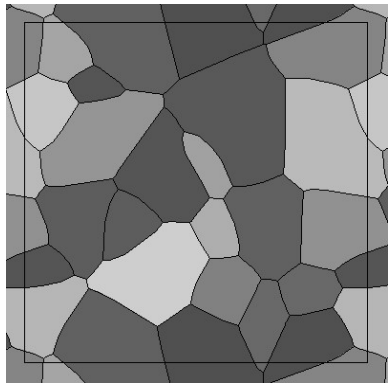

$\varepsilon = 0$

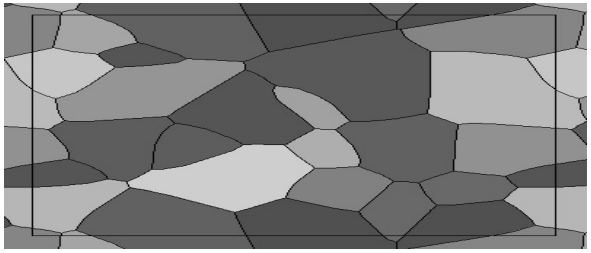

$\varepsilon = 0.5$

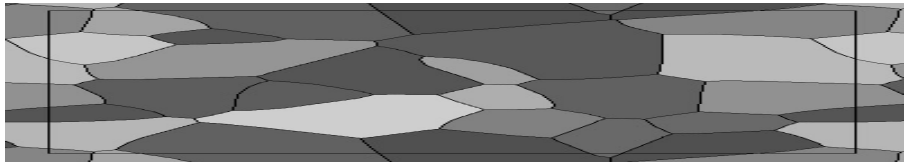

$\varepsilon = 1$

(b)

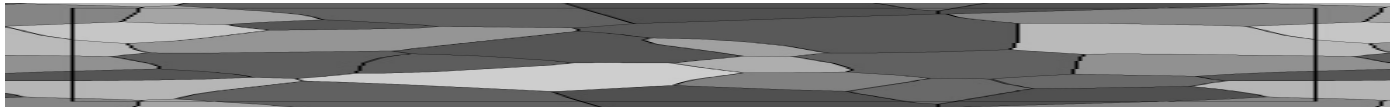

$\varepsilon = 1.5$

Figure 1

from Maurice & Humphreys [1998]

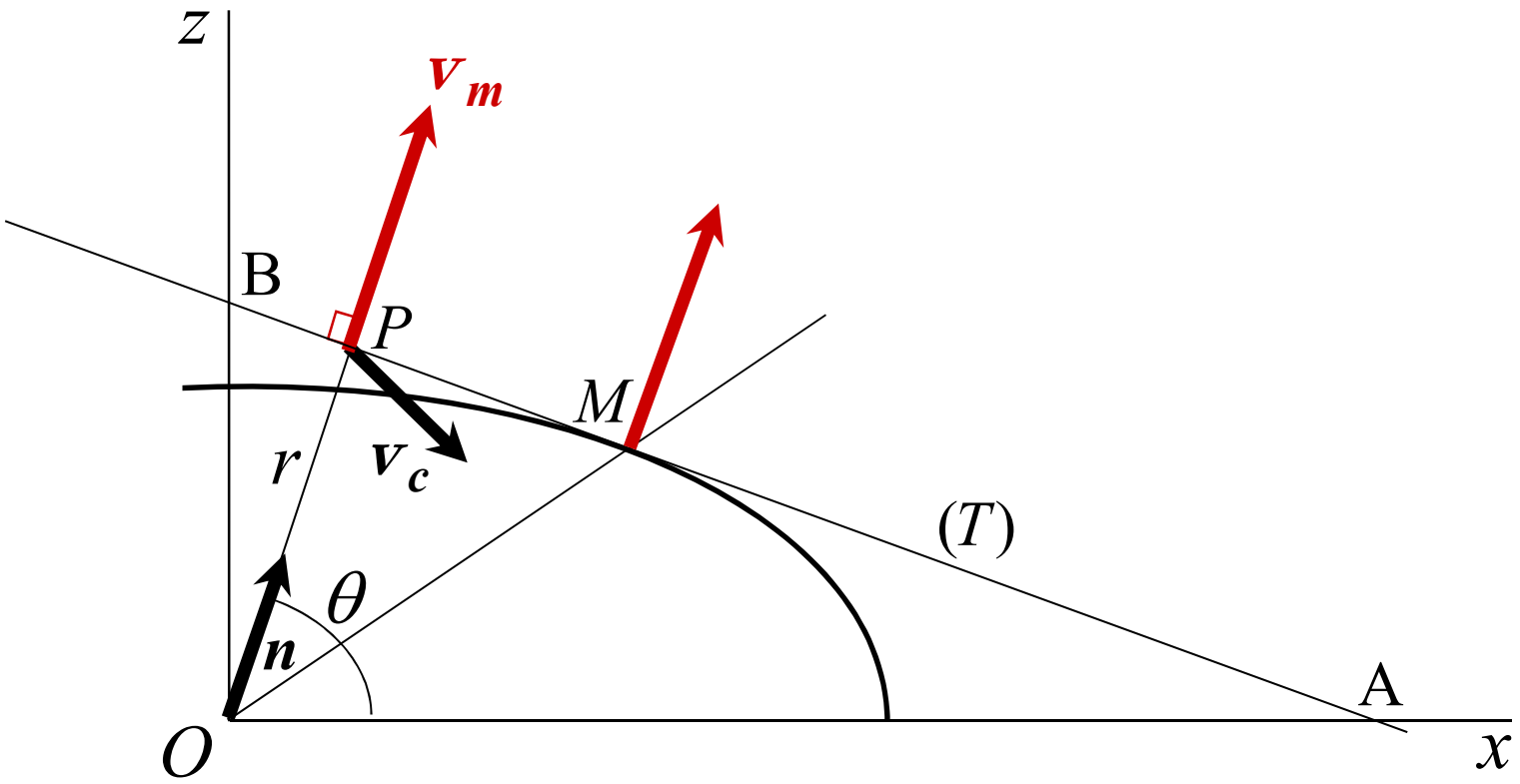

Figure 2

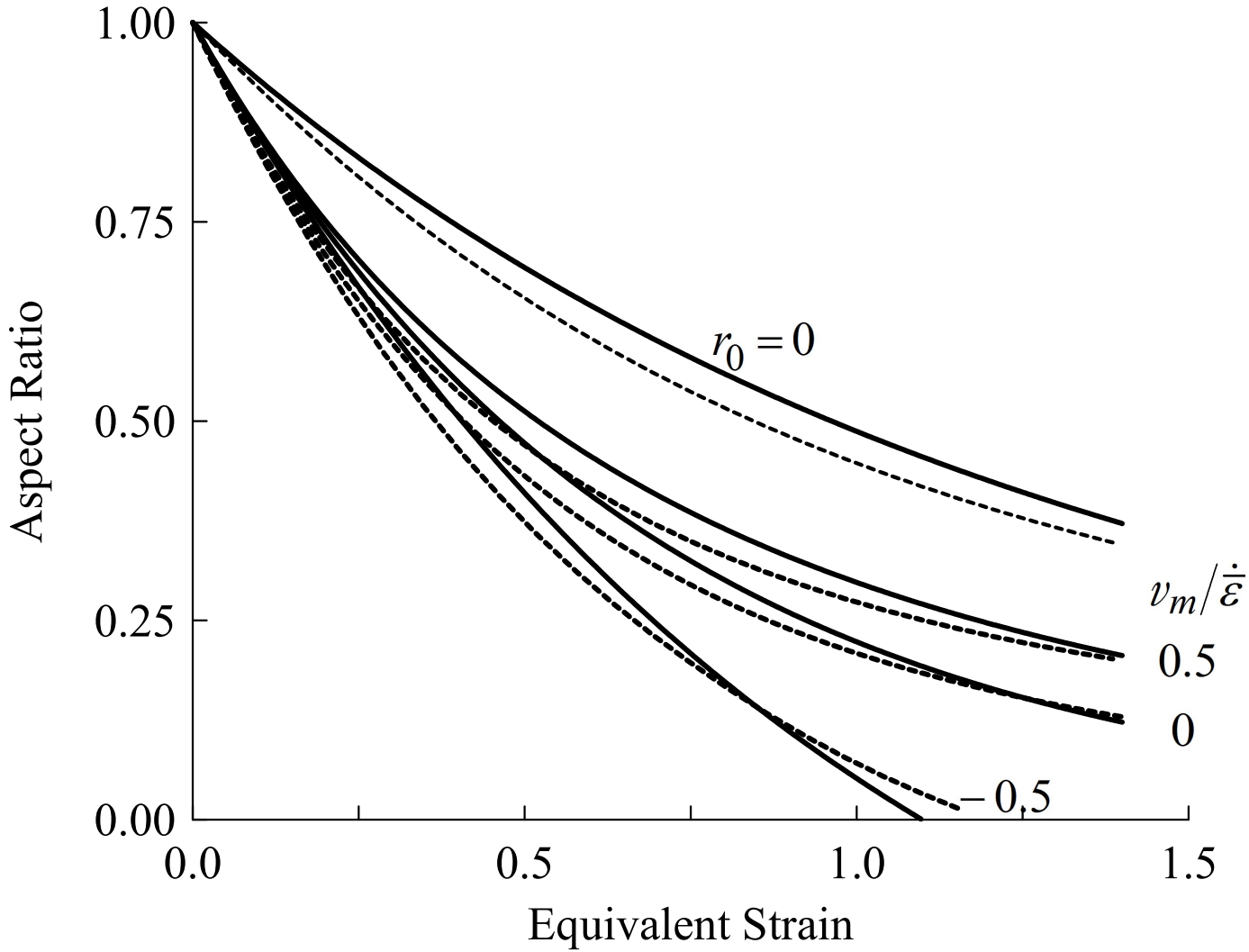
1.00
0.75
0.50
0.25
0.00
Aspect Ratio
0.0
0.5
1.0
1.5
Equivalent Strain
$r_0 = 0$
$v_m/\dot{\bar{\varepsilon}}$
0.5
0
– 0,5

Figure 3

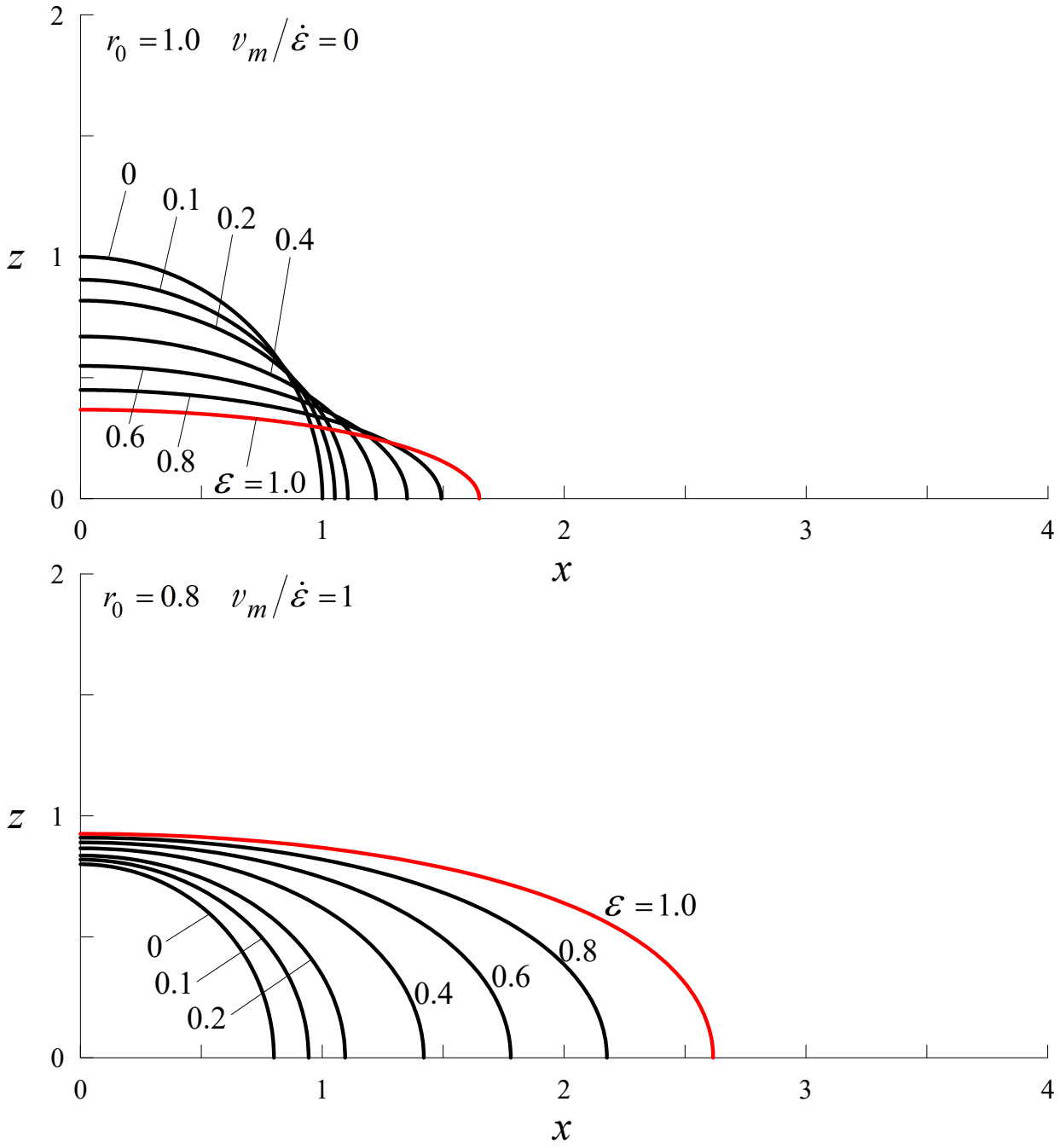
(a)
$r_0 = 1.0$ $v_m/\dot{\varepsilon} = 0$
0
0.1
0.2
0.4
0.6
0.8
$\varepsilon = 1.0$
z
x
(b)
$r_0 = 0.8$ $v_m/\dot{\varepsilon} = 1$
0
0.1
0.2
0.4
0.6
0.8
$\varepsilon = 1.0$
z
x

Figure 4

(c)

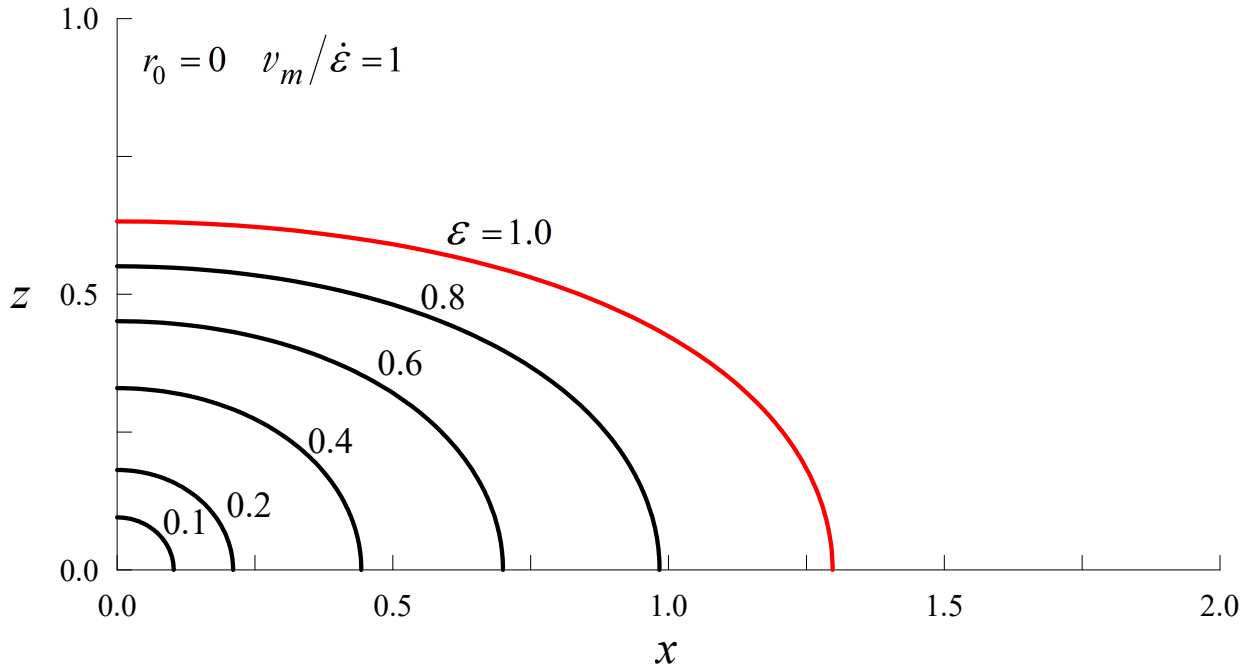
1.0
$r_0 = 0 \quad v_m / \dot{\varepsilon} = 1$
$\varepsilon = 1.0$
0.8
0.6
0.4
0.2
0.1
z
0.5
0.0
0.0
0.5
1.0
1.5
2.0
x

Figure 4

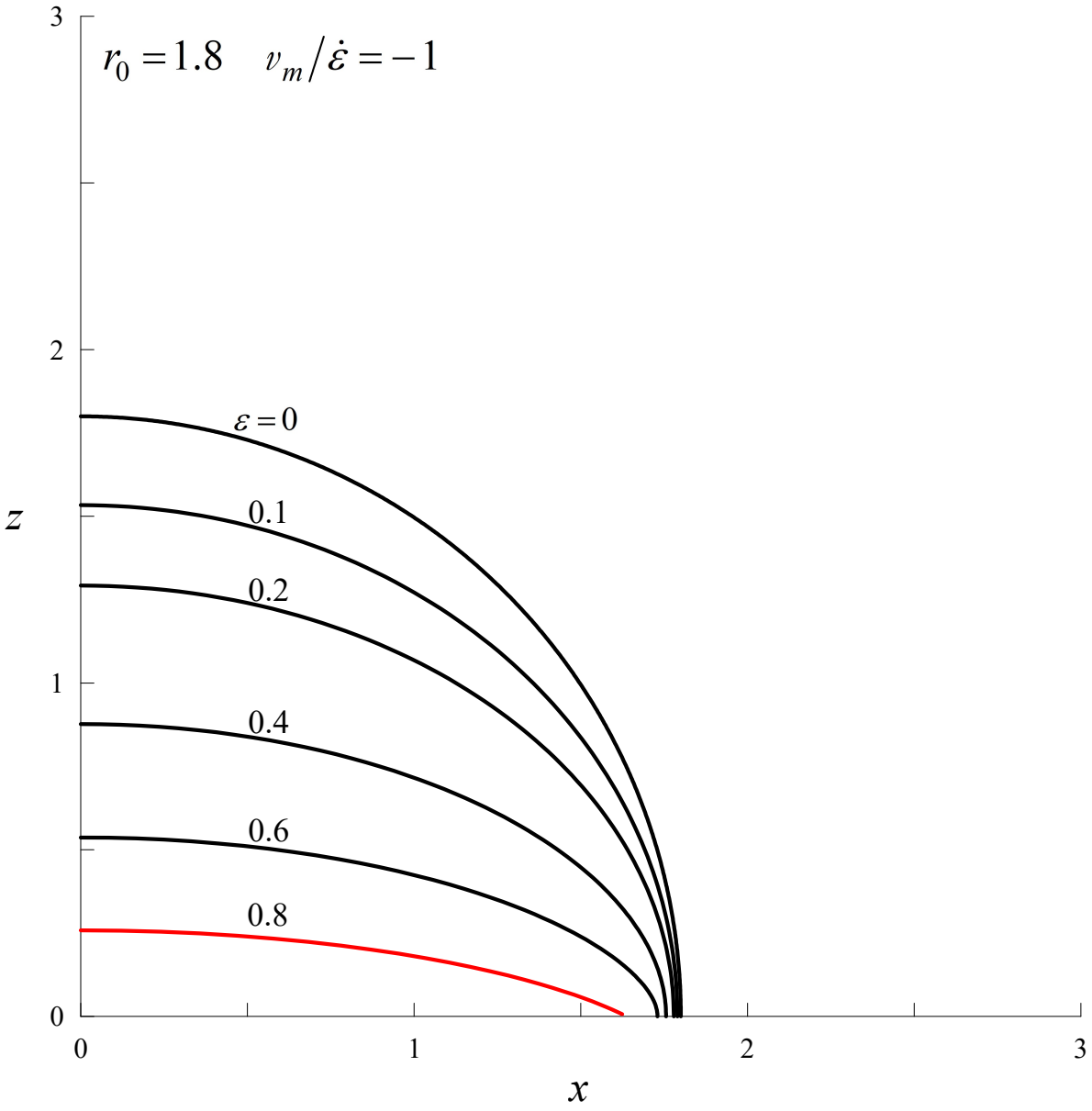
$r_0 = 1.8 \quad v_m/\dot{\varepsilon} = -1$
$\varepsilon = 0$
0.1
0.2
0.4
0.6
0.8
z
x
0
1
2
3

(d)

Figure 4

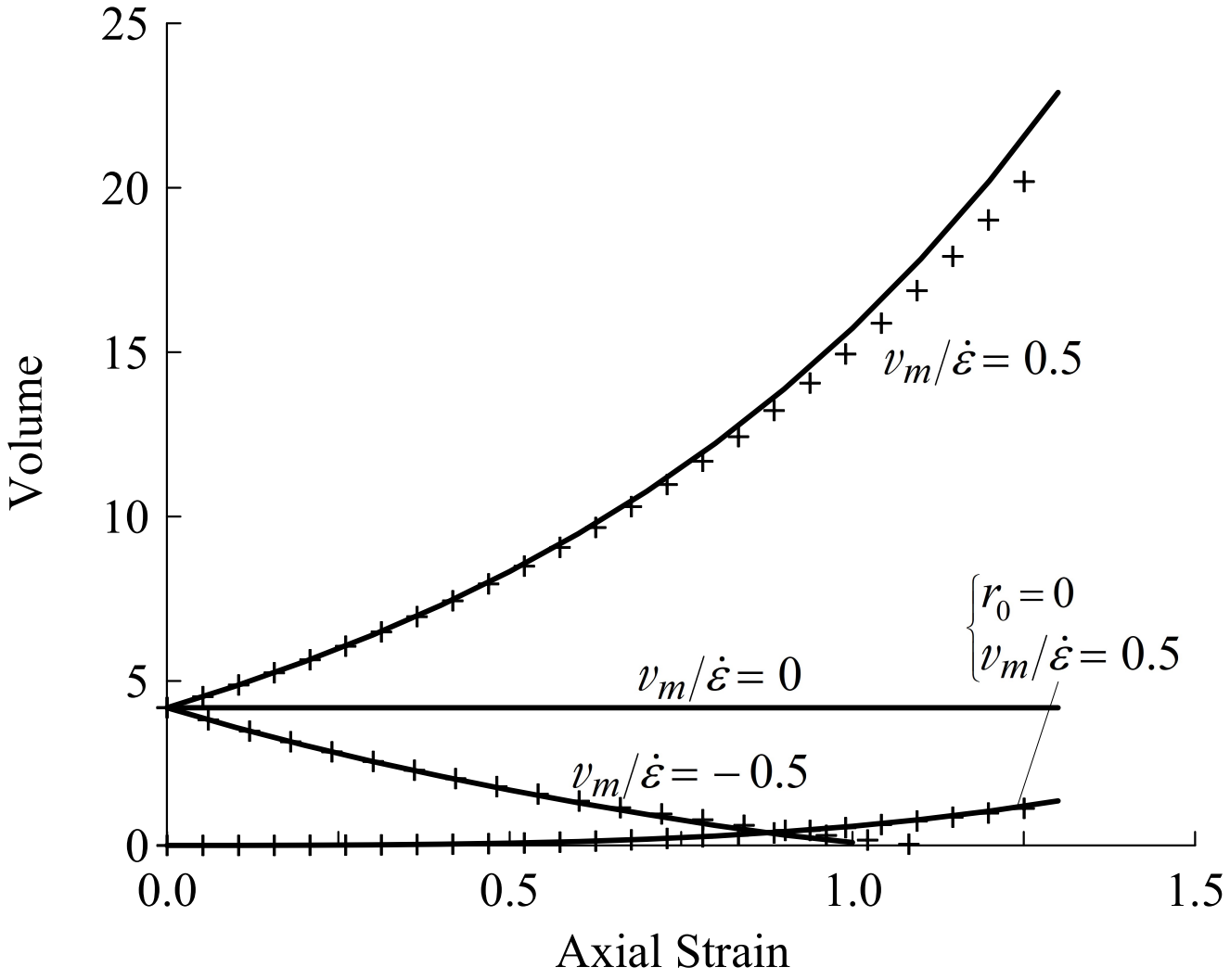
25
20
15
10
5
0
Volume
0.0
0.5
1.0
1.5
Axial Strain
$v_m/\dot{\varepsilon} = 0.5$
$\begin{cases} r_0 = 0 \\ v_m/\dot{\varepsilon} = 0.5 \end{cases}$
$v_m/\dot{\varepsilon} = 0$
$v_m/\dot{\varepsilon} = -0.5$

(a)

Figure 5

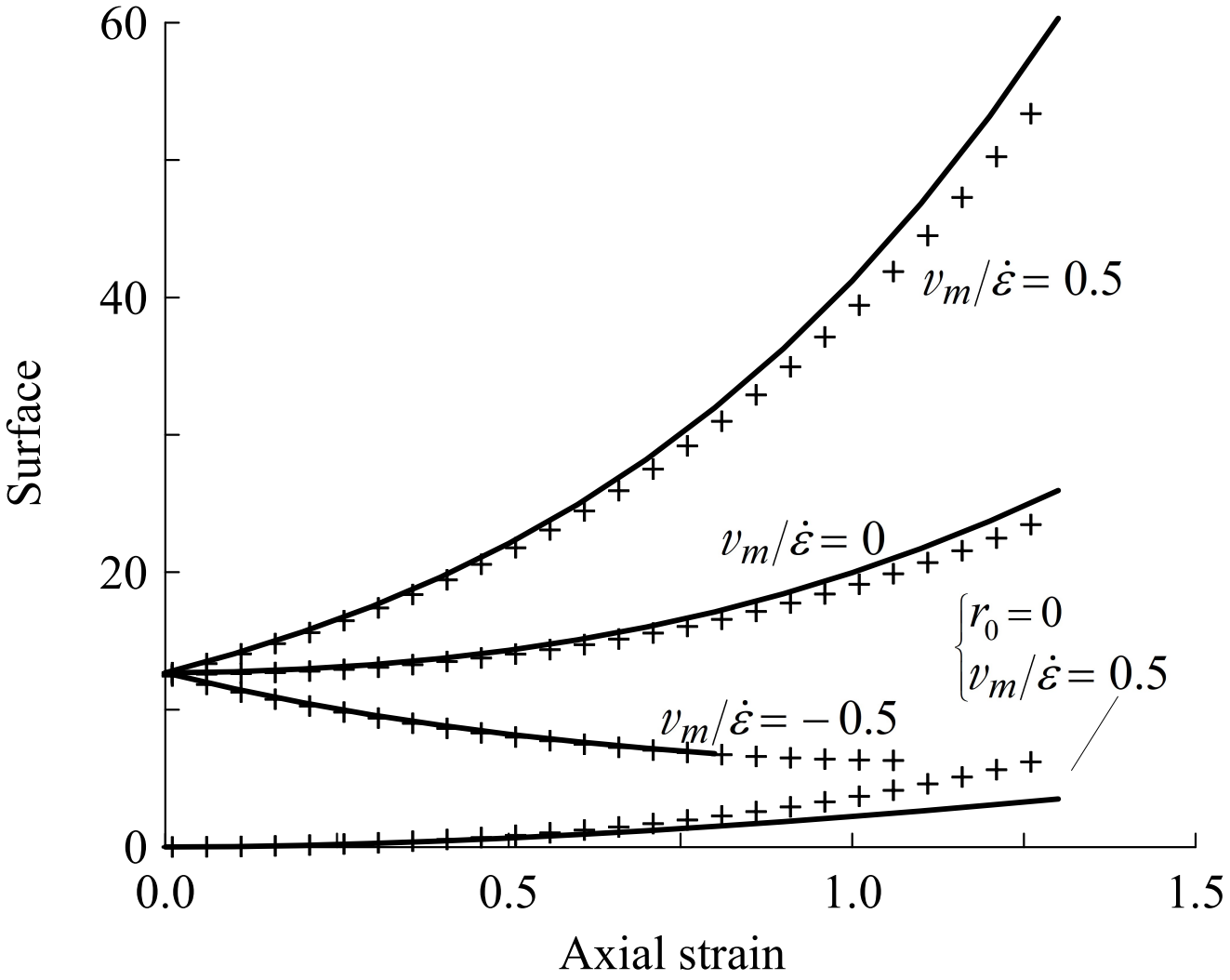
60
40
20
0
Surface
0.0
0.5
1.0
1.5
Axial strain
$v_m/\dot{\varepsilon} = 0.5$
$v_m/\dot{\varepsilon} = 0$
$r_0 = 0$
$v_m/\dot{\varepsilon} = 0.5$
$v_m/\dot{\varepsilon} = -0.5$

(b)

Figure 5

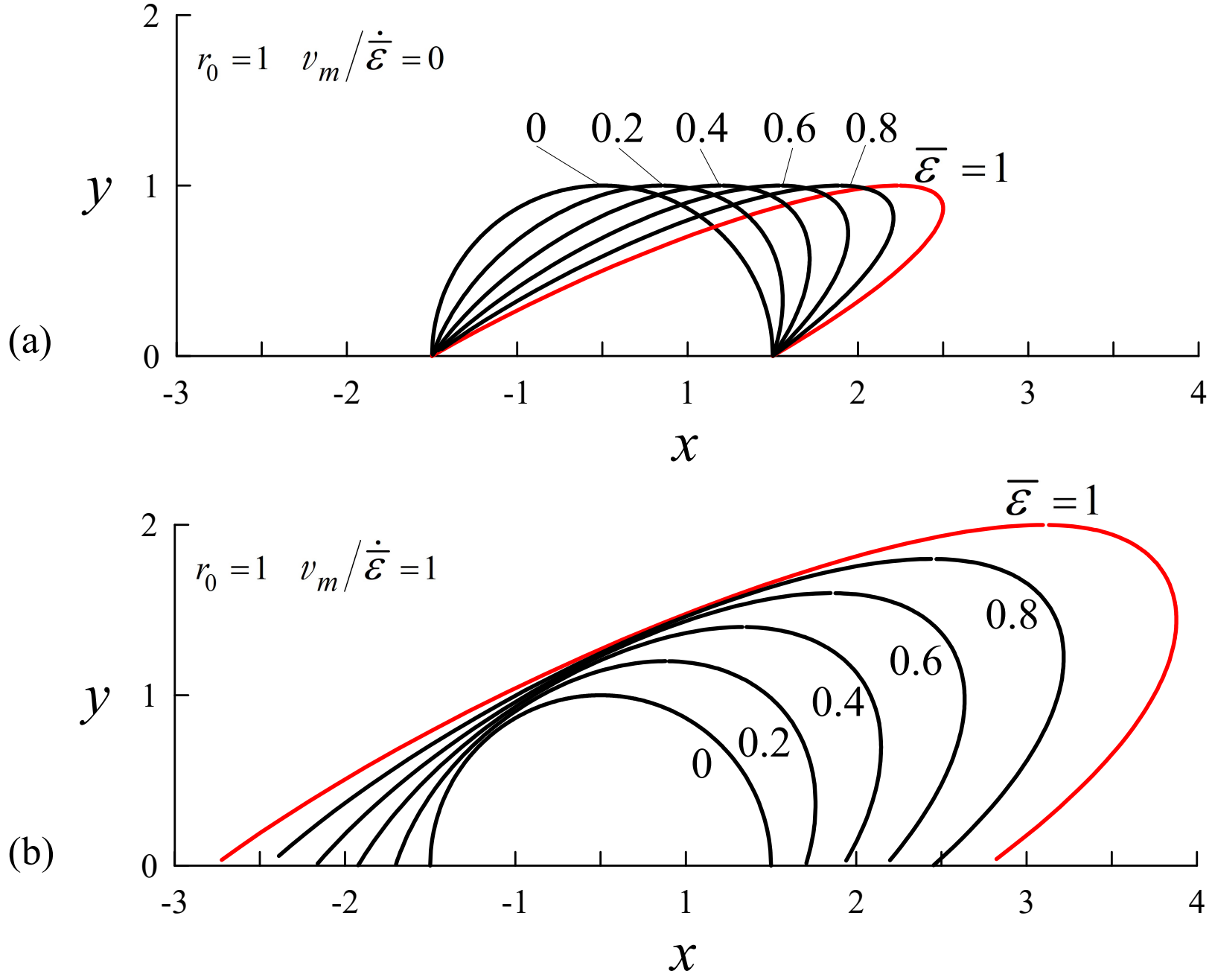
(a)
$r_0 = 1 \quad v_m / \dot{\bar{\varepsilon}} = 0$
0 0.2 0.4 0.6 0.8
$\bar{\varepsilon} = 1$
y
x
(b)
$r_0 = 1 \quad v_m / \dot{\bar{\varepsilon}} = 1$
$\bar{\varepsilon} = 1$
0 0.2 0.4 0.6 0.8
y
x

Figure 6

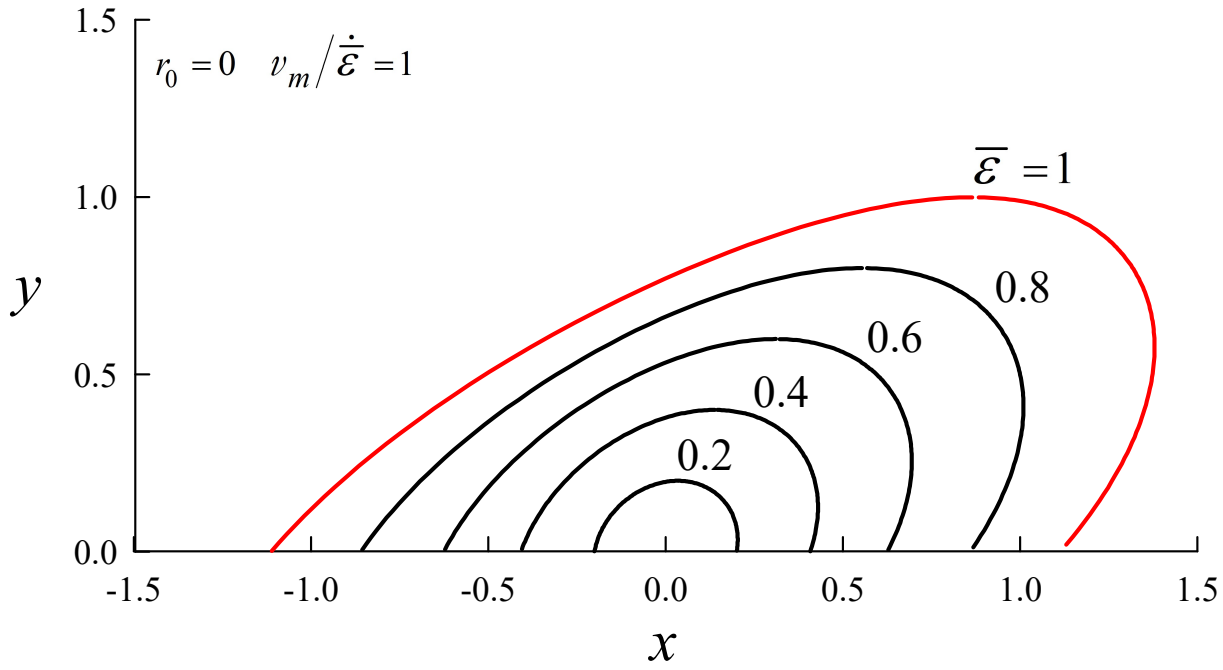
$r_0 = 0 \quad v_m / \dot{\bar{\varepsilon}} = 1$
$\bar{\varepsilon} = 1$
0.8
0.6
0.4
0.2
1.5
1.0
0.5
0.0
-1.5
-1.0
-0.5
0.0
0.5
1.0
1.5
y
x

(c)

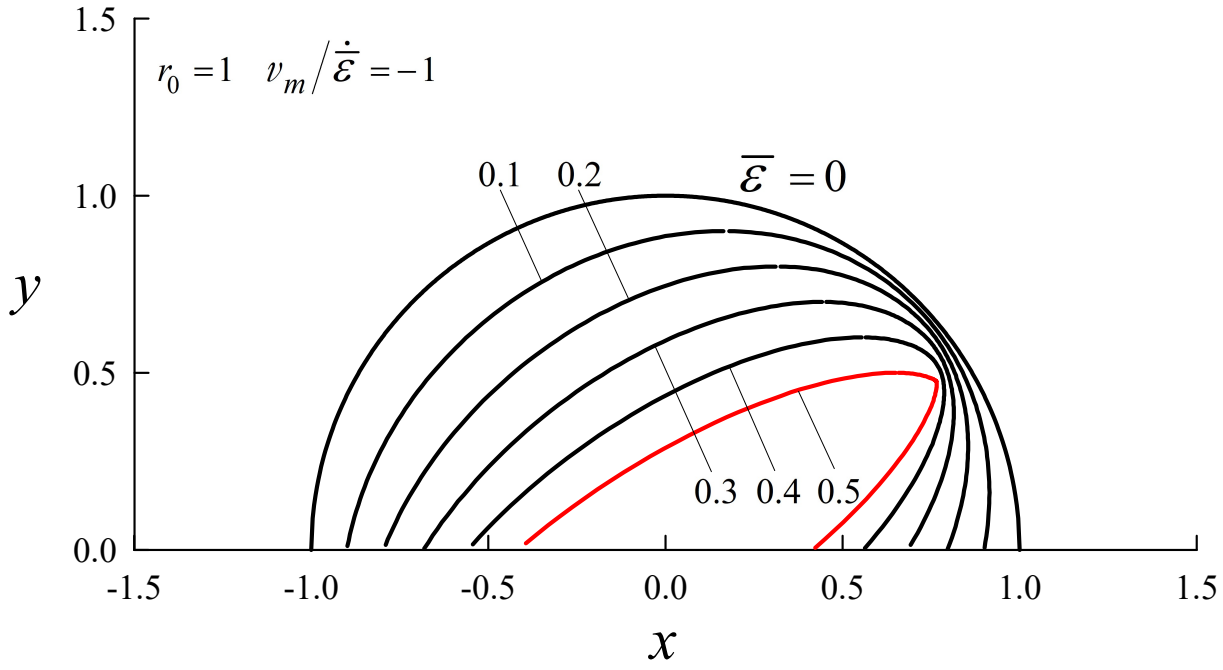
$r_0 = 1 \quad v_m / \dot{\bar{\varepsilon}} = -1$
0.1
0.2
$\bar{\varepsilon} = 0$
0.3
0.4
0.5
1.5
1.0
0.5
0.0
-1.5
-1.0
-0.5
0.0
0.5
1.0
1.5
y
x

(d)

Figure 6

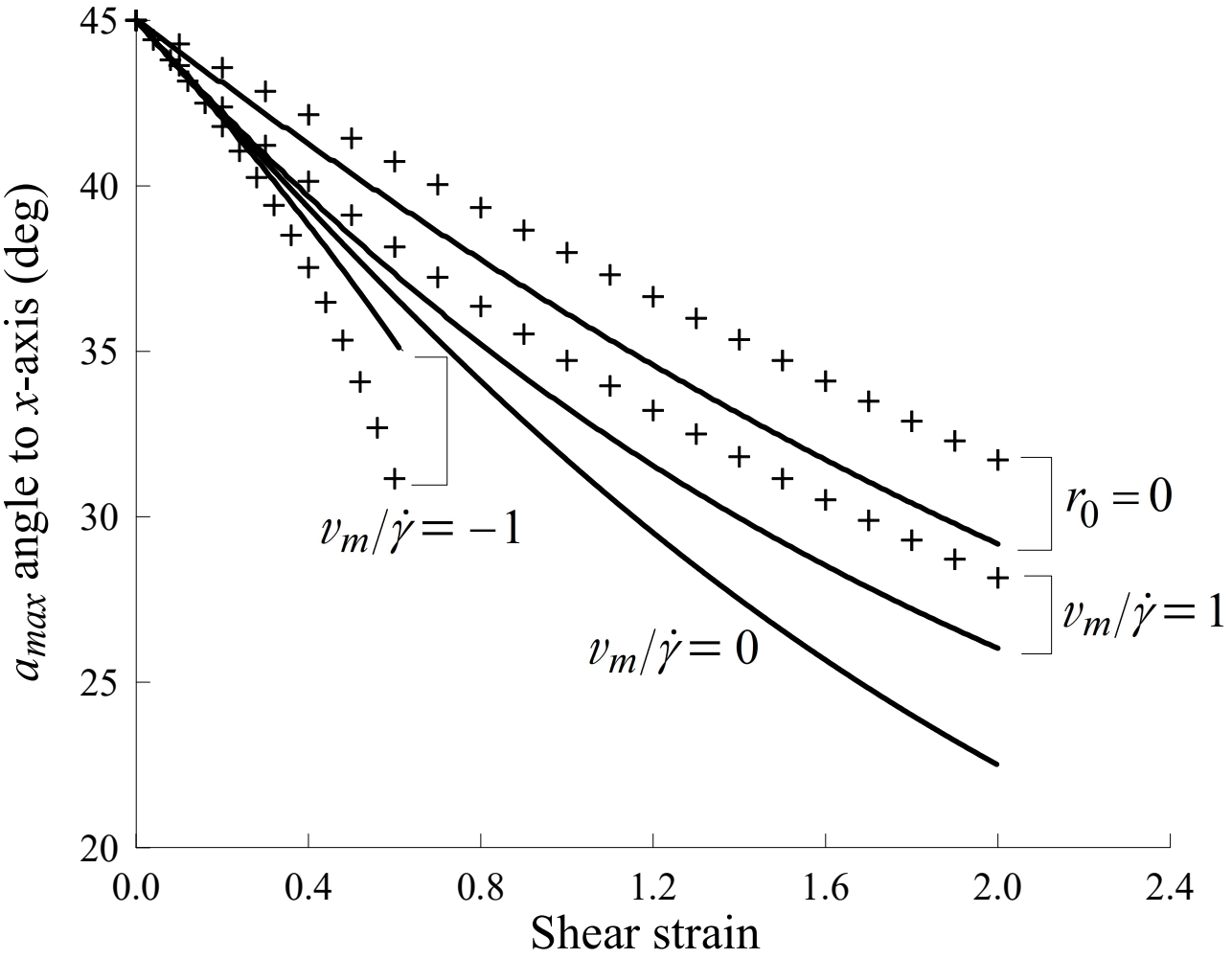
45
40
35
30
25
20
0.0
0.4
0.8
1.2
1.6
2.0
2.4
a_{max} angle to x-axis (deg)
Shear strain
$r_0 = 0$
$v_m/\dot{\gamma} = 1$
$v_m/\dot{\gamma} = 0$
$v_m/\dot{\gamma} = -1$

Figure 7

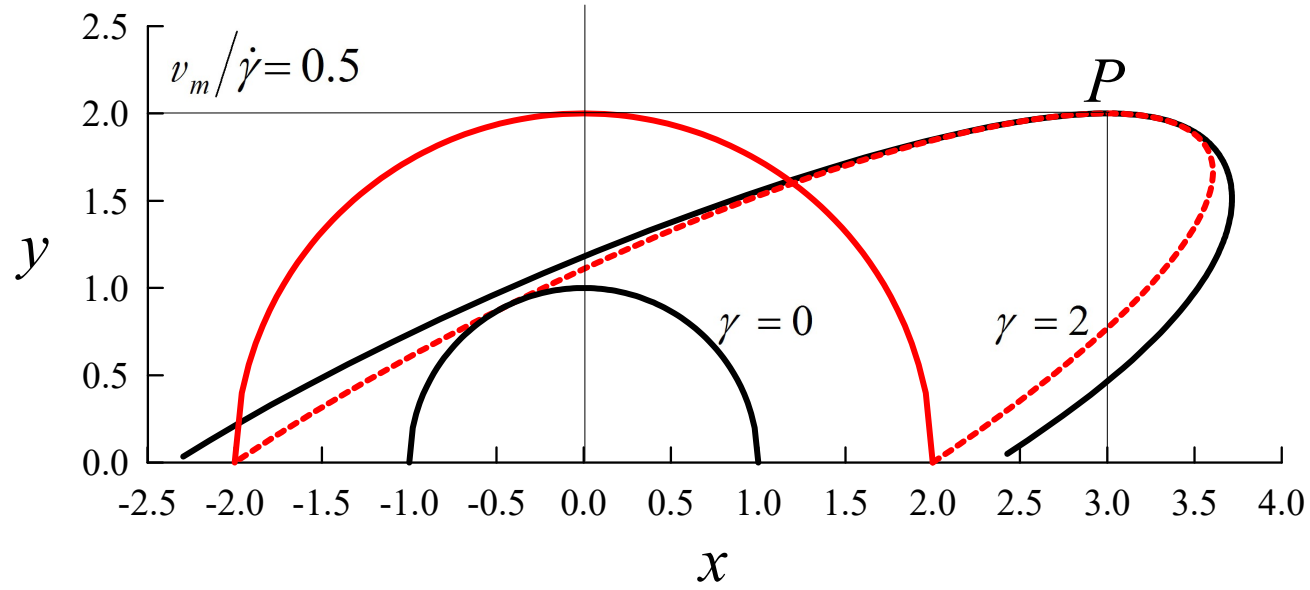
$v_m/\dot{\gamma}=0.5$
P
$\gamma=0$
$\gamma=2$
y
x
2.5
2.0
1.5
1.0
0.5
0.0
-2.5 -2.0 -1.5 -1.0 -0.5 0.0 0.5 1.0 1.5 2.0 2.5 3.0 3.5 4.0

(a)

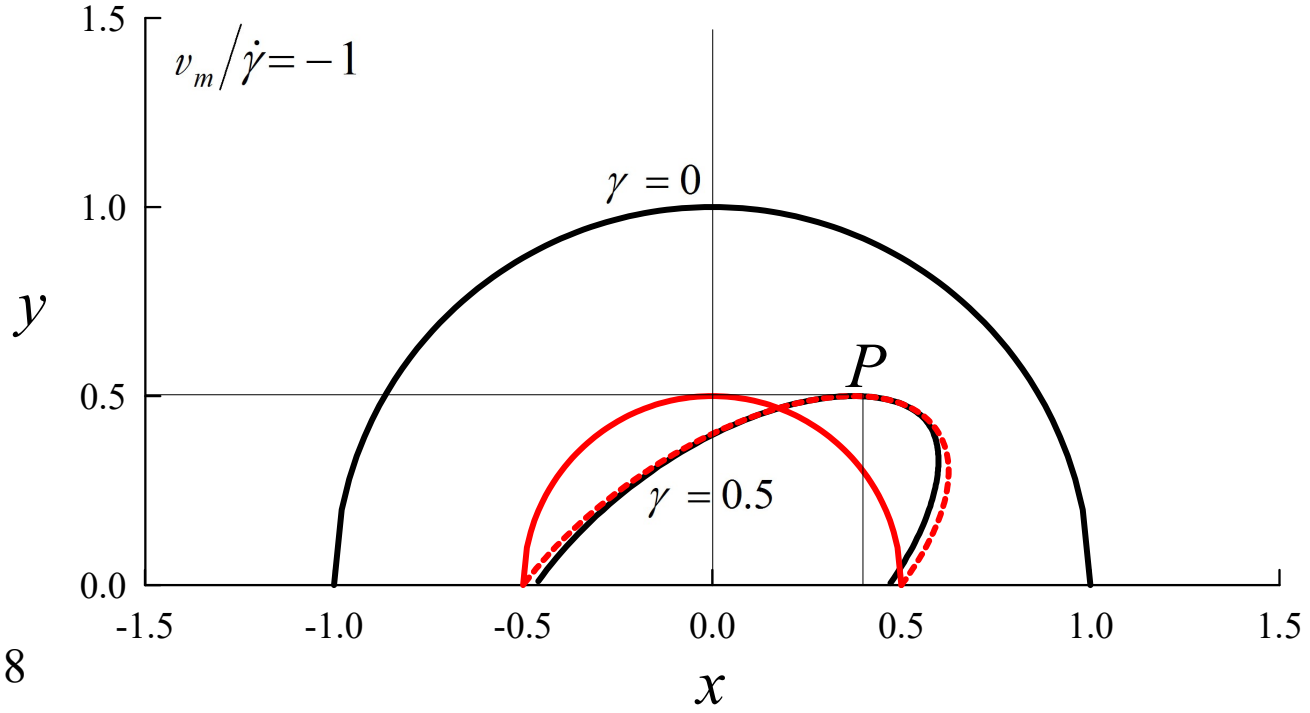
$v_m/\dot{\gamma}=-1$
$\gamma=0$
P
$\gamma=0.5$
y
x
1.5
1.0
0.5
0.0
-1.5 -1.0 -0.5 0.0 0.5 1.0 1.5

(b)

Figure 8

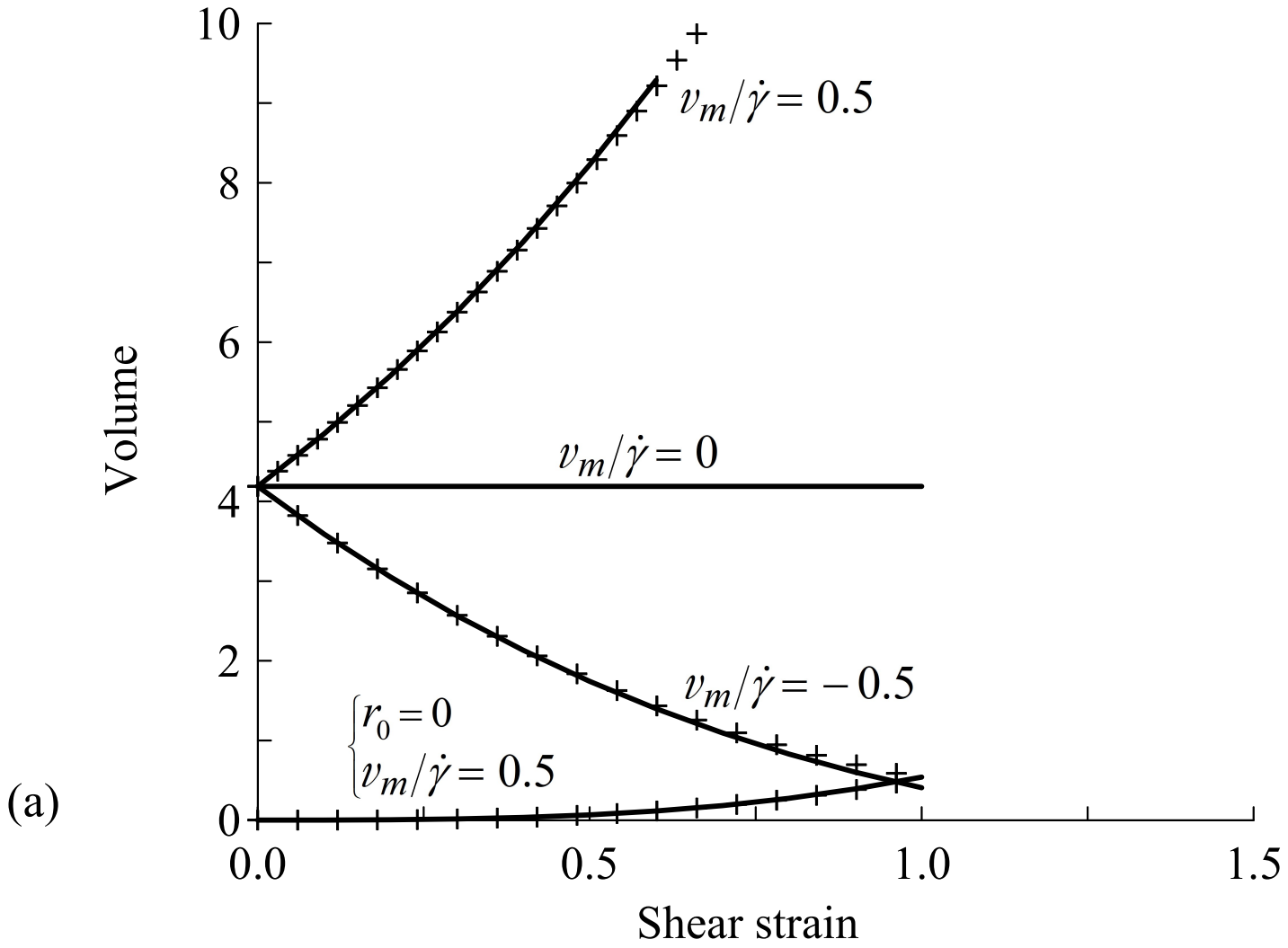
10
8
6
4
2
0
Volume
$v_m/\dot{\gamma} = 0.5$
$v_m/\dot{\gamma} = 0$
$v_m/\dot{\gamma} = -0.5$
$r_0 = 0$
$v_m/\dot{\gamma} = 0.5$
0.0
0.5
1.0
1.5
Shear strain

(a)

Figure 9

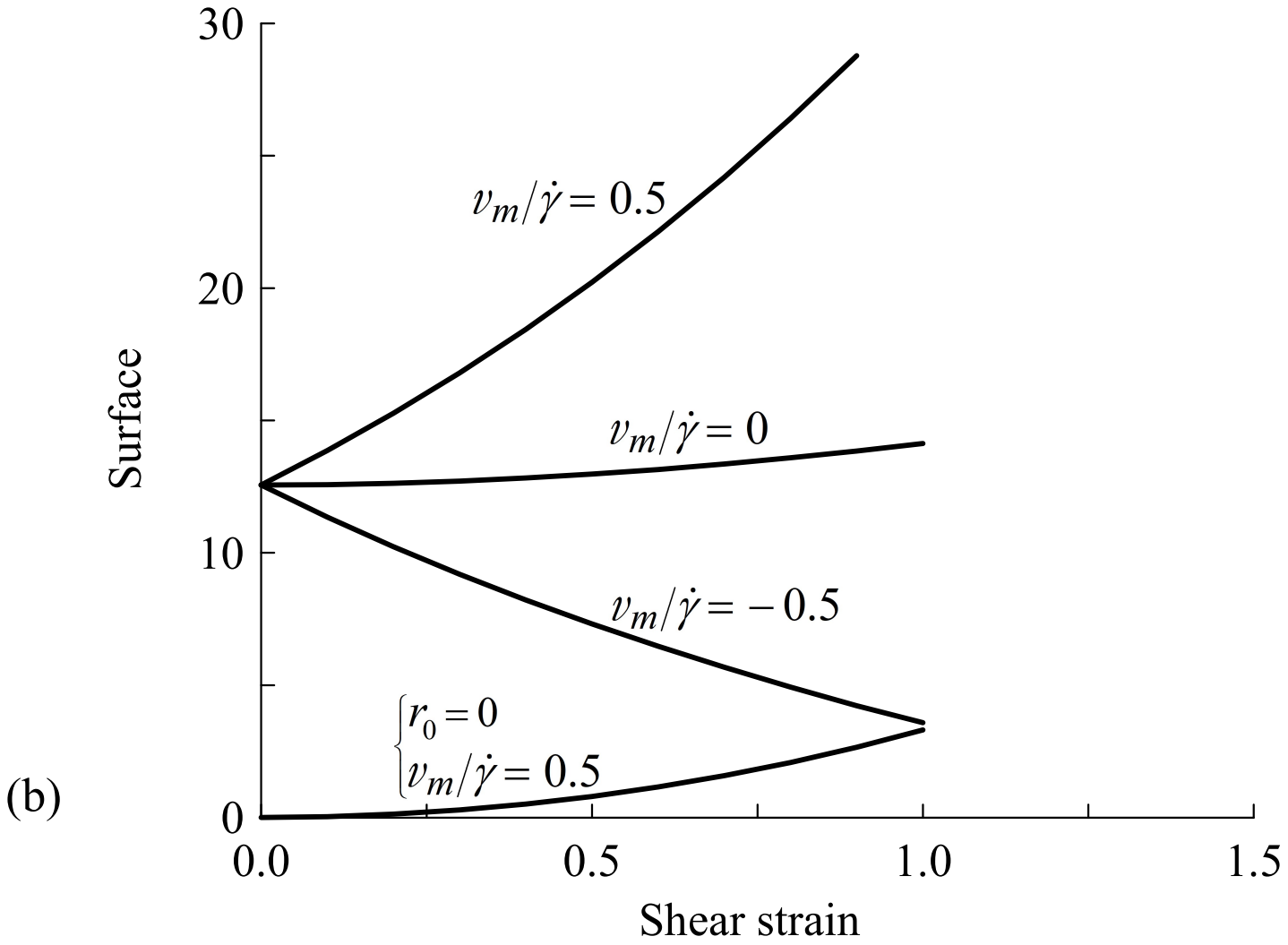
30
20
10
0
Surface
$v_m/\dot{\gamma} = 0.5$
$v_m/\dot{\gamma} = 0$
$v_m/\dot{\gamma} = -0.5$
$r_0 = 0$
$v_m/\dot{\gamma} = 0.5$
0.0
0.5
1.0
1.5
Shear strain

(b)

Figure 9

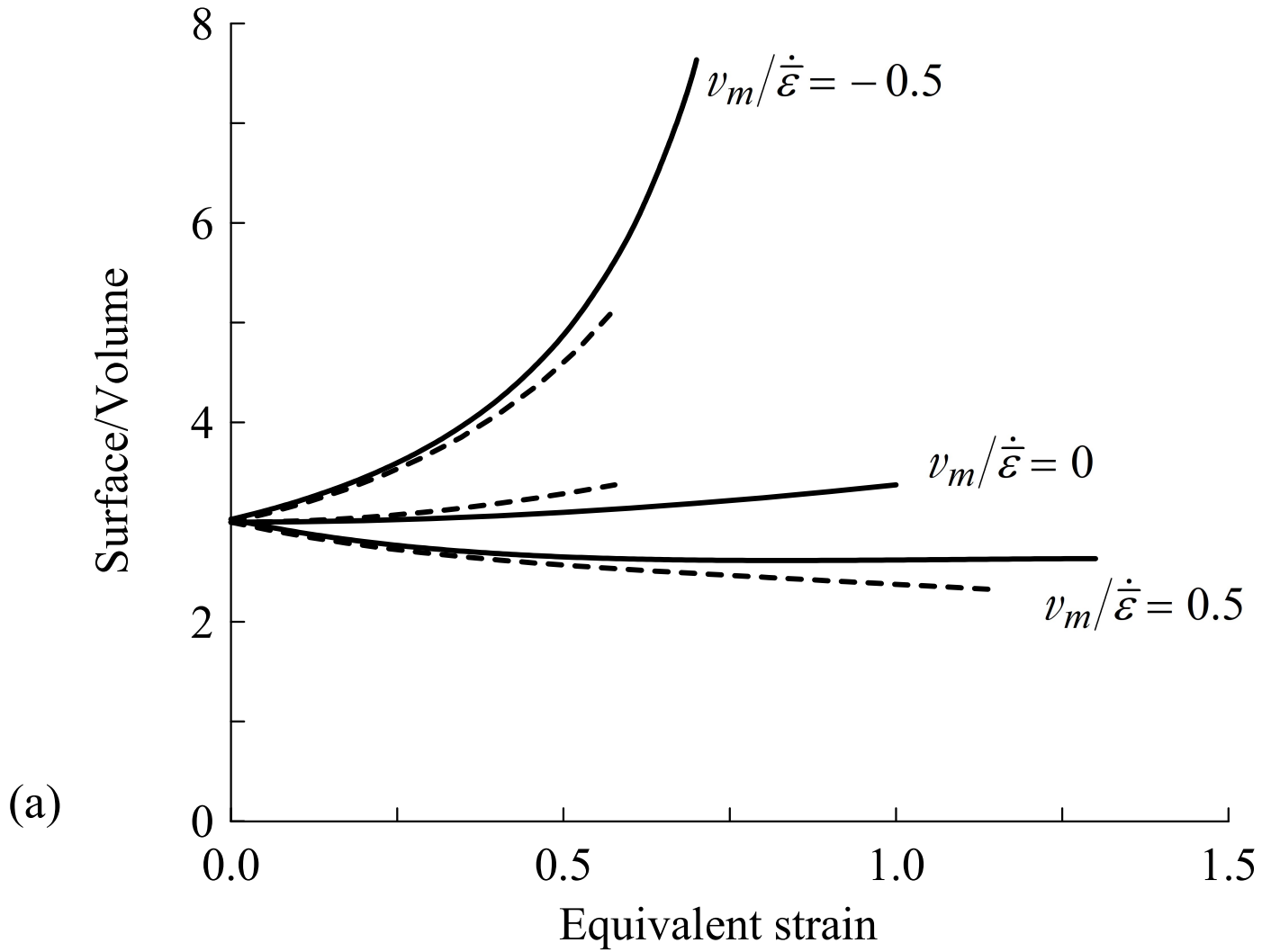
8
6
4
2
0
Surface/Volume
$v_m/\dot{\bar{\varepsilon}} = -0.5$
$v_m/\dot{\bar{\varepsilon}} = 0$
$v_m/\dot{\bar{\varepsilon}} = 0.5$
0.0
0.5
1.0
1.5
Equivalent strain

(a)

Figure 10

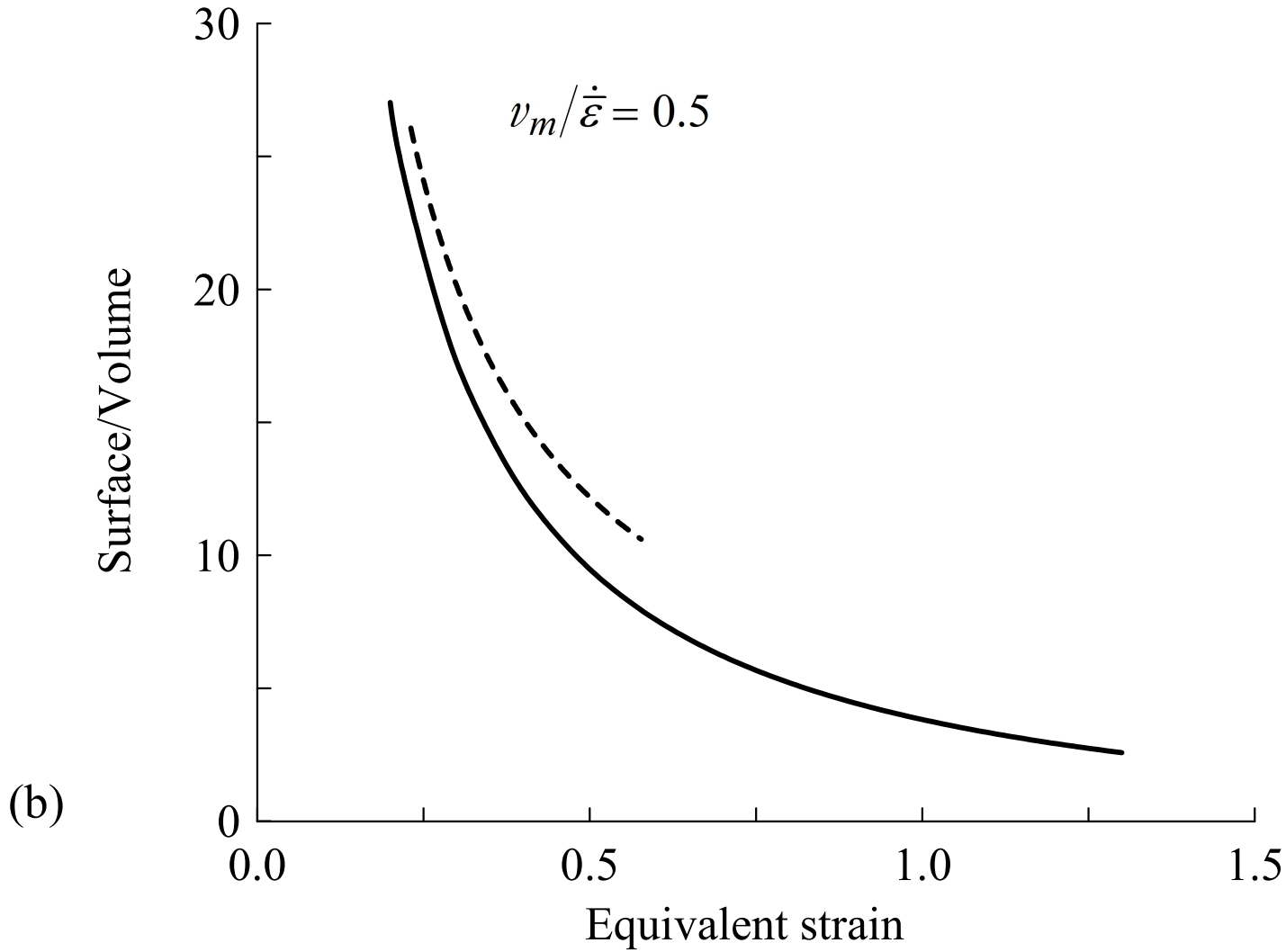
30
20
10
0
$v_m/\dot{\bar{\varepsilon}} = 0.5$
Surface/Volume
0.0
0.5
1.0
1.5
Equivalent strain

(b)

Figure 10

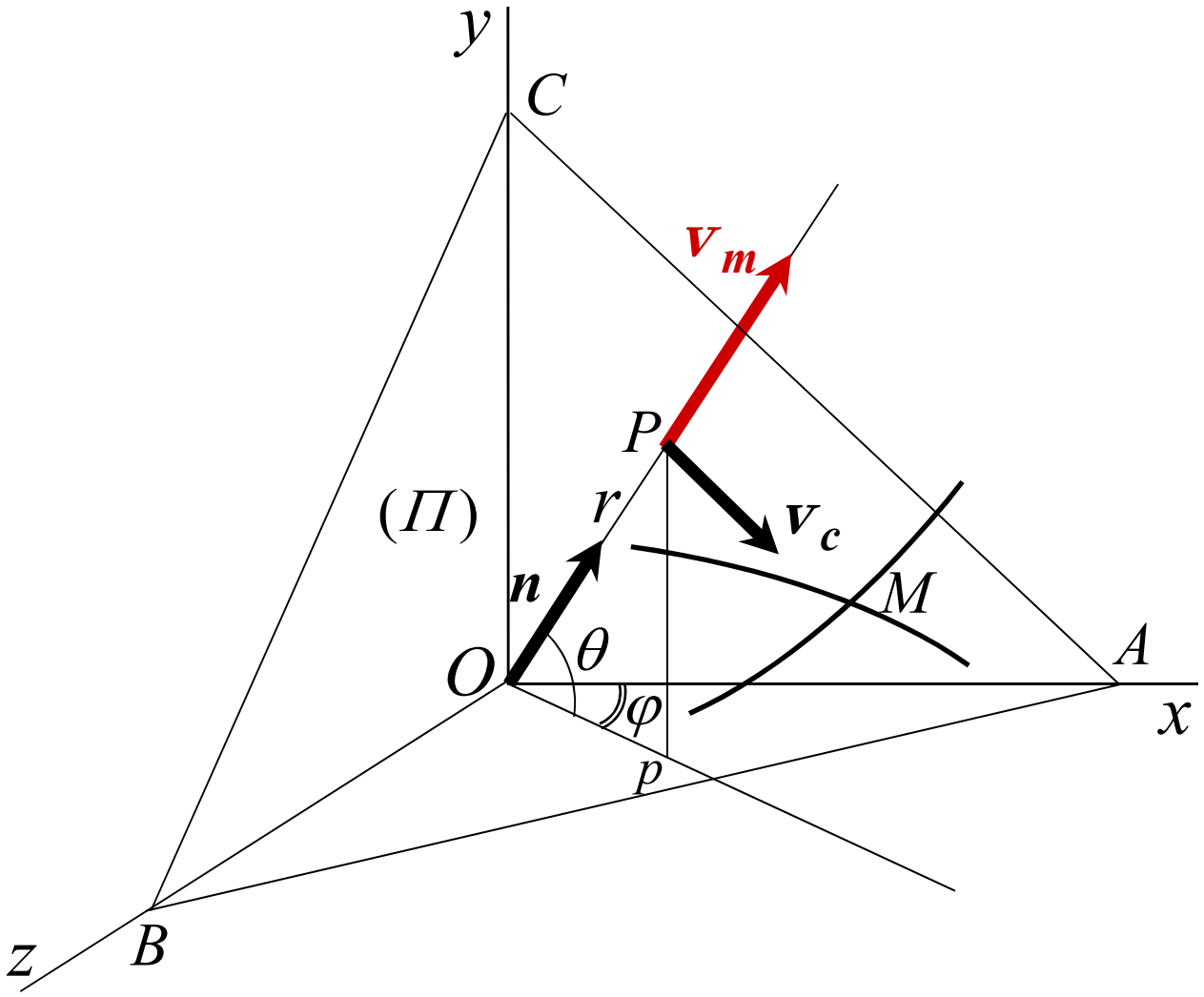

Figure B.1